CHARACTERIZATION OF CASCADE GEARBOX FOR WAVE ENERGY CONVERTERS

Jacob Ljungbäck

Master of Science Thesis MMK 2015:108 MKN 145

KTH Industrial Engineering and Management

Machine Design

SE-100 44 STOCKHOLM

Examensarbete MMK 2015:108 MKN 145

KTH Industriell teknik och management

Karakterisering av kaskadväxel för vågenergiomvandlare

Jacob Ljungbäck

Godkänt 2015-11-06	Examinator Ulf Sellgren	Handledare Stefan Björklund
	Uppdragsgivare CorPower Ocean	Kontaktperson Oscar Hellaeus

SAMMANFATTNING

Detta examensarbete utfört i samarbete med CorPower Ocean, är det slutgiltiga steget i författarens utbildning på masternivå på KTH (Kungliga Tekniska Högskolan) Stockholm. Syftet med arbetet är att karakterisera en kaskadväxellåda som används för att omvandla vertikal rörelse från vågor till rotation som driver generatorer i företagets framtida vågkraftverk samt att utifrån resultat föreslå möjliga förbättringar och belysa eventuella problem.

Den metod som använts för att karakterisera kaskadväxellådan var att via fysiska mätningar, på den testrigg placerad på KTH (Kungliga Tekniska Högskolan) i Stockholm, erhålla data för lastfördelningen i den geometriskt överbestämda konstruktionen. Dessa data användes sedan för att kalibrera en statisk och en dynamisk modell som också utvecklades för det här projektet. Huvudfokus för arbetet har legat i att ta reda på om den konstruktion som används för att fördela lasten mellan kugghjulen fungerar tillfredställande samt att säkerställa att inget kugghjul tar mer än de *2,5%* överlast vid fullast växellådan är dimensionerad för vid något tillfälle. Examensarbetet inkluderar även feltoleransers inverkan på lastfördelningen i kaskadväxeln.

Resultaten visade att den nuvarande konstruktionen presterar inom de specificerade dimensioneringsintervallen. Några oväntade karaktärsdrag upptäckdes dock vid analys av resultaten. På grund av en avsiktlig geometrisk oregelbundenhet släpade hälften av kugghjulen efter åt ena hållet vilket i sin tur resulterade i en ojämn lastfördelning och oönskade sidokrafter på kuggracken. Flexenheterna som används för att fördela lasten likvärdigt mellan kugghjulen skilde sig åt i styvhet. Den inverkan spridningen av dessa har på lastfördelningen belystes också eftersom lastfördelningen konvergerar mot värden direkt proportionella mot styvhetsförhållandet mellan dem.

Slutsatsen från examensarbetet är att den nuvarande konstruktionen, även om den fungerar tillfredställande, lämnar utrymme för förbättringar som potentiellt kan förbättra både livslängd och lastfördelningsprestanda.

Nyckelord: Dynamisk, Statisk, Modell, Kaskad, Kugghjul, Flankspel

Master of Science Thesis MMK 2015:108 MKN 145

KTH Industrial Engineering and Management

Characterization of Cascade gearbox for wave energy converter

Jacob Ljungbäck

Approved 2015-11-06	Examiner Ulf Sellgren	Supervisor Stefan Björklund
	Commissioner CorPower Ocean	Contact person Oscar Hellaeus

ABSTRACT

This Master Thesis, written in collaboration with CorPower Ocean, serves as the finalization of the author's master degree education at KTH (Royal Institute of Technology) Stockholm. The purpose has been to characterize the Cascade gearbox which is used to convert vertical motion induced by waves to rotational motion which powers generators in the company's future wave energy power plant. The purpose was also to suggest future improvements and shed light on any problems discovered.

The method for characterizing the Cascade gearbox was to conduct physical measurements of the load sharing in the inherently overdetermined geometrical design. These data were then used to calibrate a static as well as a dynamic model also developed for this thesis. Focus has been on determining that the novel load sharing method is sufficient and that no gear takes more than the *2,5%* overload during max load the gearbox is dimensioned for at any time. Also included in the thesis is an analysis of the tolerances effect on the performance of the Cascade gearbox.

Results showed that the current design perform within the expected dimensioning limits. However some unexpected characteristics were discovered after analysis of the results. Because of deliberate geometric decisions half of the gears trail behind initially in one direction causing uneven load sharing and unwanted lateral forces on the rack. Also discovered was the importance of equal stiffness of the flex units, used to divide the load evenly between the gears, since the load sharing factor converges towards values directly proportional to the stiffness ratios in between them.

As a conclusion it can be said that although the current design is sufficient, there is still room for improvements which could enhance life expectancy as well as load sharing performance of the Cascade gearbox.

Keywords: Dynamic, Static, Model, Cascade, Gear, Backlash

FOREWORD

In this chapter the authors own reflections and thoughts are given room. Also included are greetings to persons important for the completion of this project.

I the author would like to thank CorPower Ocean and all its employees for the opportunity to work on such an inspiring project and all the support crucial for the completion of this thesis. A special thank you goes to my industrial supervisor Oscar Hellaeus for all the help during the entire process as well as your role as counterpart during countless discussion. Also a big thank you to KTH (Royal Institute of Technology) in Stockholm for a great couple of years during my studies and to my supervisor Stefan Björklund for many useful tips especially about *MATLAB* modelling and for his guidance and support through this entire project. Lastly I thank family and friends for their support and patience during this time.

Jacob Ljungbäck

Stockholm, November-2015

NOMENCLATURE

In this chapter important notations and abbreviations are presented along with their meaning and unit.

Notations

Symbol	Description
$\vec{A}$	Gearbox direction (-)
$\vec{B}$	Gearbox direction (-)
C	Damping matrix (N/m^2)
D	Difference between ranks (-)
E	Young´s modulus (Pa)
E_{pu}	Pith deviation tolerance (m)
E_r	Gear runout tolerance (m)
F	Force (N)
H	Heaviside function
J	Moment of inertia (kg)
K	Stiffness matrix (N/m)
LS	Load sharing (-)
M	Mass matrix (kg)
N	Number of iterations (-)
Q	Gear accuracy class (-)
R	Ranks for X_{mag} (-)
S	Ranks for Y_{mag} (-)
T	Torque (Nm)
X	Displacement vector (m)
b	Backlash (m)
d	Diameter (m)
e	Pitch deviation error (m)
g	Piecewise relative displacement with backlash (m)
h	Contact constraint (-)
k	Stiffness (N/m)
k^θ	Rotational stiffness (N/deg)
l	Length (m)
m	Mass (kg)

m_n	Gear Module (mm)
p	Relative gear mesh displacement (m)
q	Gear radius in relative gear mesh for gear ratio (-)
r	Radius (m)
t	Time (s)
w	Gear mesh frequency (Hz)
x_j	Displacement of gear j (m)
ε	Position of gear pitch deviation (rad)
$\hat{\rho}$	Spearman rank correlation (-)
θ	Rotational displacement (deg)
φ	Phase angle (rad)
ψ	Gear position angle (rad)
ϕ	Monte Carlo simulation (-)
Superscripts	
h	Contact constraint is included
θ	Indicates rotational stiffness
Subscript	
a	Alternating force vector
b	Backlash alternating force
e	Error alternating force
j_1	Driving gear
j_2	Driven gear
$j_{1,2}$	Interaction between gear j_1 and j_2
m	Mean input force vector
Abbreviations	
FE	Finite element
GUI	Graphical User Interface
LVDT	Linear variable displacement transducer
ODE	Ordinary differential equations
WEC	Wave Energy Converter
G1x	Gear name: first gear after pinion
G2x	Gear name: second gear after pinion
G3x	Gear name: third gear after pinion
G4	Gear name: fourth gear after pinion
px	Gear name: pinion
r	Gear name: rack

TABLE OF CONTENTS

1 INTRODUCTION

In this chapter background information to wave energy as well as the problem description, purpose and delimitations is presented along with the method used to characterize the Cascade gearbox.

1.1 Background

The force of the ocean and more specifically the force of the waves have inspired inventors as early as two centuries ago to attempt to utilize that power for human benefit (Falnes, 2007). However when fossil fuels, such as petroleum, became the most important means of power in the early 20th century, further development of wave-energy halted (Falnes, 2007). After the oil crisis of the 1970s, wave-energy was once again on researcher's radar. This meant the start of modern research on the subject (Hals, 2010) and a number of research initiatives were initiated (Clément et al., 2002). When price of petroleum declined in the 1980s further development was once again halted due to reduced funding (Falnes, 2007) but the field returned once again after the start of the new millennium (Hals, 2010). Even though interest in wave-energy historically somewhat fluctuates depending on petroleum availability, it remains a significant potential source of sustainable energy (Vicinanza et al., 2013). It is estimated that the global power potential of waves hitting all coasts worldwide is in the order of 10^{12} *W* and in the order of 10^{13} *W* if that energy is harvested out on the open ocean, the latter in the same quantity as the present global power consumption (Falnes, 2007).

Despite this immense unexploited source of energy an insignificant part of the world's generated power originates from wave-energy, EIA (2012). This is largely due to profitability difficulties in the sense that no previous technology has proven efficient enough given the expense (Hals, 2010).

CorPower Ocean utilizes a new invention called a Cascade gearbox to convert the vertical motion induced by a buoy floating on the surface of the ocean to rotational motion which powers generators more efficiently and in a smaller package than before. By using phase control and a method derived from latching invented in 1980 by Budal and Falnes (Babarit et al., 2004), which sets the buoy in resonance with the waves, combined with the Cascade gearbox CorPower Ocean expects to be able to extract up to five times as much energy as the competition at one third of the price, CorPower Ocean (2012).

1.2 Purpose

Since the Cascade gearbox is a new invention, knowledge of its actual behavior is limited. Important factors such as load sharing due to its inherent over determination and the dynamic effect of tolerances are virtually unknown. This master thesis aims at proposing a method to model the gearbox in a way that gives solid quantitative results of its performance which in turn may serve as a basis of the solutions feasibility. Important results to determine are the forces in each gear, the load sharing between the eight pinion wheels and the winding of the compliant load sharing mechanisms. A static as well as dynamic model was developed in *MATLAB*. In order to verify and calibrate the models, physical measurements was conducted. In addition to already stated deliverables sufficient data for lifetime calculations are provided to enable future work along with the possibility to use the models for future analysis of the tolerances effect on

the load sharing. In this specific case the Cascade gearbox is modelled in scale 1:2 to correspond with the contemporary test rig located at KTH (Royal Institute of Technology), Stockholm.

1.3 Delimitations

Since models considering every aspect of the gearbox would generate work exceeding the timeframe given to this project some limitations and simplifications had to be made in order to scale down the task to a more suitable size. These are as follows;

- Load sharing mechanisms are modeled as one rotational/translational spring element.
- Vibrations are not considered.
- Losses are not considered.
- The gear house is considered infinitely stiff and solid.
- The gear rack is assumed to be perfectly centered.
- The model includes the gearbox from input to flywheel.
- No lifetime or stress calculations are included. However sufficient data to enable such calculations of the flex units in the future are provided.

1.4 Method

The method used to characterize the gearbox was a three step process starting with a static model based on classical gear contact mechanics. From that a dynamic differential equation model was developed to further improve simulated data. Lastly physical measurements were carried out to verify and calibrate the two aforementioned models.

The chosen software for the modelling of the gearbox is, as stated in a previous section, *MATLAB*. This since it provides the necessary ability to customize the calculations and include a tolerance chain analysis based on a Monte Carlo simulation. Analytical models are commonly used in order to model gear interactions e.g. (Moradi and Salarieh, 2012), (Chen and Wu, 2009) and (Kahraman, 1999). Other commonly used methods are Multi Body Simulation usually with ADAMS e.g. (Zhu et al., 2014) alternatively a FE analysis in optional software e.g. (Kahraman et al., 2003) and (Fernandez et al., 2013). However these models often demand vast amounts of computing power (Bodas and Kahraman, 2004) and usually only cover gear interactions in one stage.

For the physical measurements pre-existing LVDT sensors registering the angle of each compliant mechanism were installed and used. These were tested for functionality along with the stiffness of each rubber bushing in the compliant mechanisms prior to installation.

1.5 Report disposition

The main disposition of this report follows, in many ways, the order described previously in Method. Detailed description of the disposition is as follows;

1. Introduction
2. Frame of reference
3. The process
4. Results
5. Discussion and conclusion
6. Recommendations and future work

The **Introduction** chapter describes the background, purpose, delimitations and method used in this master thesis project. In **Frame of reference** important theory and technical knowledge are presented to the reader for improved understanding of the thesis. **The process** describes how the static and dynamic models as well as the physical measurements were set up and implemented. In **Results** important graphs, resulting forces and the corresponding load sharing of each pinion gear from both models and physical measurements are presented along with matching results from the statistical tolerance analysis. **Discussion and conclusion** consists of a thorough discussion of the feasibility of each assumption and all results presented in this thesis as well as conclusions drawn with respect to results acquired. Finally in **Recommendations and future work** suggestions for improvements and further development will be discussed.

2 FRAME OF REFERENCE

In this chapter necessary theory and technical knowledge are presented aiming at improving the understanding of the reader.

2.1 Cascade gearbox

A Cascade gearbox is a new invention patented by CorPower Ocean, see Figure 1. It is related both to a planetary gear and a rack and pinion in the sense that it serves as a combination of the two. The largest benefit is the ability to transfer high loads during high speeds in a lightweight package and with high efficiency. Contrary to conventional use of gearboxes, CorPower Ocean utilizes the Cascade gearbox to increase speed rather than decreasing it.

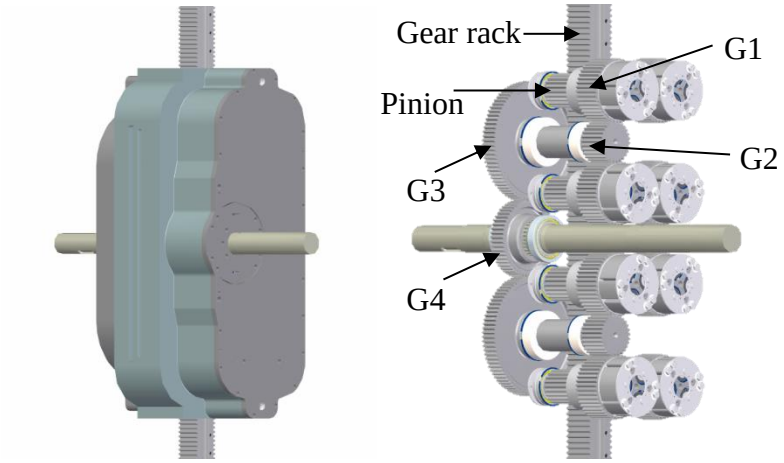

Figure 1. The cascade gearbox displayed with cover (left) and without (right).

The Cascade gearbox consists of a rack which drives eight pinion gears, four on each side of the rack. Connected to the pinion wheels via a shaft and a compliant flex mechanism are a larger set of spur gears, hereafter known as G1 gears, mounted in pairs i.e. one of the G1 gears drives the other. Power is further transmitted from the G1 gear pairs to another set of smaller spur gears, hereafter known as G2 gears, which connects two pairs of G1 gears. Mounted directly to the G2 gears via a shaft are the largest sets of spur gears, hereafter known as G3 gears, which transmit power to a single output gear, hereafter known as G4 gear which connects two groups of identical sets of four pinion gears, see Figure 2. The two gear ratios of the gearbox are between the G1 and G2 gears and between the G3 and G4 gears. Mounted to the same shaft as G4 is a flywheel denoted, as f in the models as well as a generator.

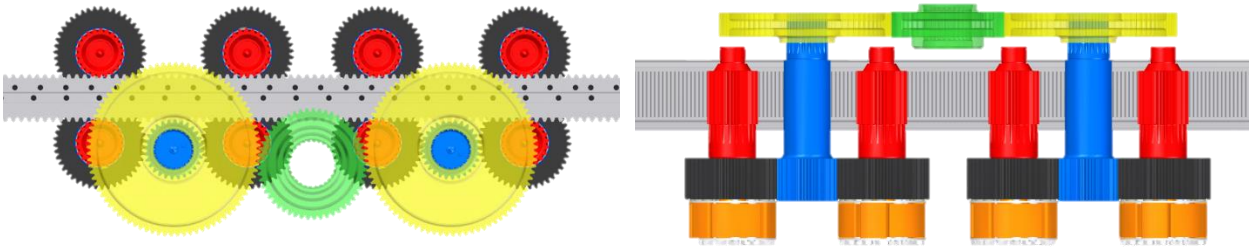

Figure 2. A schematic overview of the Cascade gearbox. Power is transmitted from the rack (grey) to the eight pinions (red). Power is then transferred via a flex unit (orange) and a shaft to the G1 gears (black) and then to the G2 gears (blue) which in turn transfers the power via a shaft to the G3 gears (yellow). Finally power is transferred to the G4 gear (green).

Since the load of the rack is distributed between eight pinion wheels it is possible to use smaller pinions without sacrificing load carrying capacity. This results in lighter and less costly pinions with the added positive side effect of higher rotational speed which is beneficial when powering a generator.

The design of the cascade gearbox does however cause some problems for the contact of the gear pairs. Firstly Pinion 1 can force Pinion 2 to spin freely i.e. cause the gap between the rack and Pinion 2 to remain unchanged and vice versa. This is the case if one of the pinions are in contact with the rack and G11 and G12 are in contact before the other pinion are in contact with the rack, see Figure 3. The same problem can occur in every gear contact in the gearbox. However when the pinion that causes the free spin has closed its power route to gear G4 i.e. closed every gear gap from the rack to the output gear, it can no longer cause another gear to spin freely.

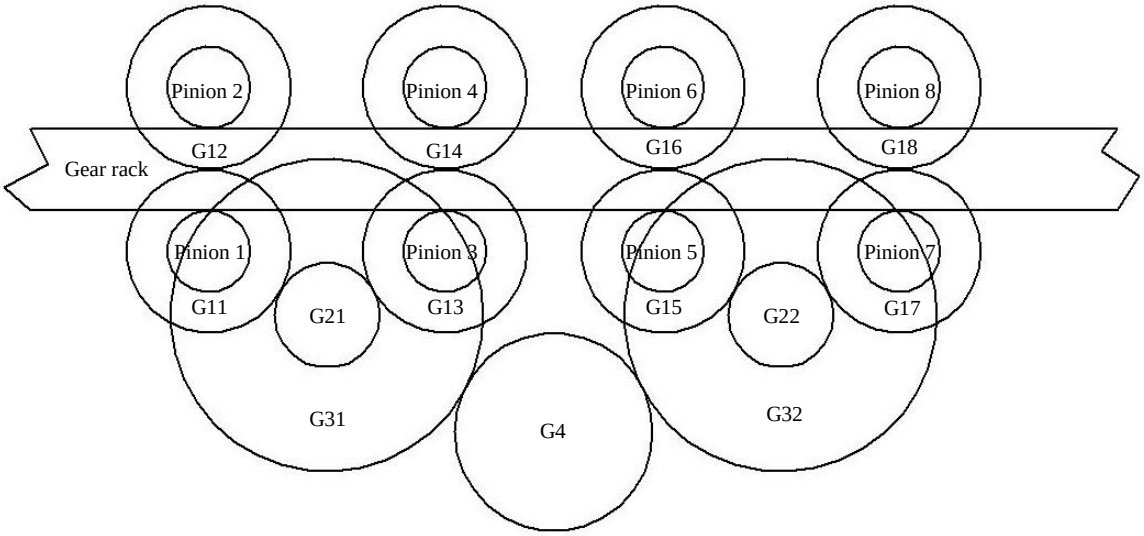

Figure 3. Schematic picture of the Cascade gearbox with names of all gears.

If power is transferred backwards, i.e. a gear that is supposed to be driven by another gear is actually driving the other, gear gaps can increase rather than decrease This is however only a hypothetical scenario since it requires abnormal tolerance errors to ever occur.

Because of deliberate geometrical decisions introduced to the gearbox when it is operated in one direction the two different directions have been analysed separately. The direction without the geometric difference is from now on known as direction $\vec{A}$. The other direction with the geometric difference is from now on known as direction $\vec{B}$.

2.2 Tolerance stackup analysis

Tolerance stackup analysis is used to calculate the cumulative effect of tolerances for a part or assembly (Fisher, 2011). Depending on complexity either a statistical or worst-case approach can be used however a general rule of thumb is that a statistical method is more accurate as the number of tolerances increase (Oberg et al., 2008) since the likelihood of all tolerances being at their maximum or minimum in every instance is highly unlikely (Fisher, 2011). A tolerance stackup analysis is performed by adding up tolerances to find the resulting tolerance range, see Figure 4.

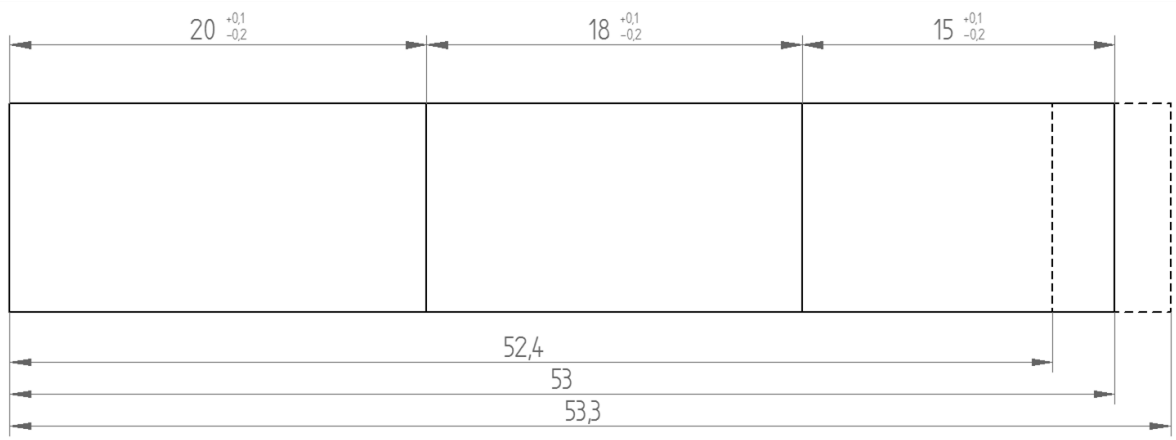

Figure 4. A tolerance stackup analysis is conducted by adding up all tolerances in a chain to find the resulting tolerance range. In this example the actual length of the object could be both longer and shorter than its nominal value.

2.3 Monte Carlo simulation

A statistical method often presents a more accurate representation of the actual system then a worst case method since the sum of all tolerances on a manufactured product most likely will approximate a normal distribution (Fisher, 2011). Monte Carlo simulation is a statistical method commonly used for computer based tolerance analysis (Fisher, 2011). Even though it is one of the most popular tools for statistical tolerance analysis, it requires larger computational time then other techniques (Somvir et al., 2012). The fundamental idea of Monte Carlo simulation in tolerance analysis is to create a statistical distribution based on several iterations N where each parameter is assigned a random value within their range, derive a result, save and then repeat the process (Fisher, 2011). The equation describing the Monte Carlo simulation of a definite parameter is given by

$$\phi = \frac{x_{\max} + x_{\min}}{2} + \mathbb{R} \cdot \frac{x_{\max} - x_{\min}}{2n} \tag{1}$$

where x_{max}, x_{min} is the maximum and minimum tolerance limits, $\mathbb{R}$ is a vector with N number of random values ranging from -1 to 1 and n determines how large portion of the generated tolerances will fall within their limits. A larger number of iterations increase the precision of the result proportional to the square root of N (Somvir et al., 2012).

2.4 Spearman rank correlation

Spearman rank correlation is a non-parametric test to determine the association between data (Dunn and Clark, 2009) and is one of the most widely known measures of correlation due to its ease of computation and simplicity (Woolson and Clarke, 2002). It was originally proposed by

Charles Spearman and builds upon preceding work by Pearson (Spearman, 1904) but has since then been slightly changed (Kvam and Vidakovic, 2007). The idea is to rank each data sample based of its magnitude, X, followed by assignment of additional ranks for each parameter contributing to the data sample based on the variables individual magnitude, Y, (Woolson and Clarke, 2002). The correlation $\hat{\rho}$ is displayed in a range from 1 to -1. A correlation of 1 indicates a large positive association and a correlation of 0 indicates a small association between that specific variable and the result of the data sample. In the same way -1 indicates a large negative association (Kvam and Vidakovic, 2007). The mathematical expression to determine Spearman's rank correlation coefficient is defined according to (Kvam and Vidakovic, 2007) as

$$\hat{\rho} = \frac{\sum_{i=1}^{n}(R_i - \bar{R})(S_i - \bar{S})}{\sqrt{\sum_{i=1}^{n}(R_i - \bar{R})^2 \cdot \sum_{i=1}^{n}(S_i - \bar{S})^2}} \tag{2}$$

where n is the number of samples, $R_1, \dots, R_n$ are the ranks for X and $S_1, \dots, S_n$ are the ranks for Y. If D is defined as the difference between ranks, i.e., $D_i = R_i - S_i$ and $\bar{R} = \bar{S}$ from $\bar{R} = \sum_{i=1}^{n} R_i/n$ and $\bar{S} = \sum_{i=1}^{n} S_i/n$ a simplified expression for Spearman's rank correlation coefficient is given according to (Woolson and Clarke, 2002) by

$$\hat{\rho} = 1 - \frac{6\sum_{i=1}^{n} D_i^2}{n(n^2-1)}. \tag{3}$$

In tolerance stackup analysis Spearman's rank correlation is useful to determine a tolerance's significance thus indicating on which individual tolerance to focus additional efforts. A brief example of the Spearman rank correlation is presented in Table 1.

Table 1. An example of Spearman's rank correlation. Each row represents a data sample, X and Y are the data components and R_i and S_i are the ranks for X and Y respectively.

X	R_i	Y	S_i	${D_i}^2$
9	3	10	1	4
2	1	40	2	1
7	2	50	3	1
			$\hat{\rho} = 1 - \frac{6\sum_{i=1}^{n} D_i^2}{n(n^2-1)}$	-0,5

3 THE PROCESS

In this chapter the structure and set up of the static as well as the dynamic and physical measurements are presented together with the tolerance analysis.

3.1 Tolerance analysis

A tolerance analysis is vital to understand and evaluate the workings and performance of the Cascade gearbox since it is inherently overdetermined. If it was possible to manufacture every component with non-existent errors to its nominal value the load sharing between the pinions would be perfect even without flex mechanisms since gear gap could virtually be removed. However since it is impossible to consistently manufacture something close enough to its nominal value to call it perfect, errors will be introduced in the design ultimately leading to unequal gaps between gear pairs. In order to obtain good representations of the tolerances effects a statistical approach, and more specifically a Monte Carlo simulation was used since the probability or risk of a worst case scenario is close to non-existent (Fisher, 2011). In this, all tolerances where assumed normally distributed and added up using tolerance stackup according to (Fisher, 2011). From this large collection of simulated tolerance errors adjusted for probability, random errors for each individual gear interaction were picked to implement in the models. This to simulate a production line where there is a small probability of picking the worst case. By doing so percentage values of how many gearboxes that would not clear the requirements were acquired.

In order to determine the significance of each tolerance in every tolerance stackup, Spearman's rank correlation coefficient was used. However further analysis of the tolerances impact on the performance of the cascade gearbox is not part of this thesis.

Apart from the dimensional tolerances from the placement of the shafts there are the gear tolerances. The gear tolerances used in this tolerance analysis are the pitch deviation E_{pu}, which is the difference between the actual and theoretical pitch between gear teeth, and gear runout E_r, which is the difference between the real and theoretical radial flank position of teeth, defined according to (Jelaska, 2012) as

$$E_{pu} = \left(0,3m_n + 1,25\sqrt{d}\right) \cdot 2^{0,5(Q-5)} \tag{4}$$

$$E_r = \left(0,24m_n + \sqrt{d} + 5,6\right) \cdot 2^{0,5(Q-5)} \tag{5}$$

where m_n is the gear module, d is the gear diameter and Q is the gear accuracy grade. All tolerances are translated to pitch deviation since that is what will affect the load sharing performance of the Cascade gearbox.

3.2 Stiffness measurements

The manufacturer of the flex units specifies a vague stiffness which meant some tests had to be conducted in order to verify the stiffness of the flex units. These tests were conducted with the flex units mounted to the gearbox to avoid complete disassembly of the gears. The test followed the test procedure of the manufacturer as close as possible. To simulate a load on the flex

mechanism an arm and calibrated weights were used, see Figure 5. The known torques was then used to calculate the rotational stiffness of the complete flex unit.

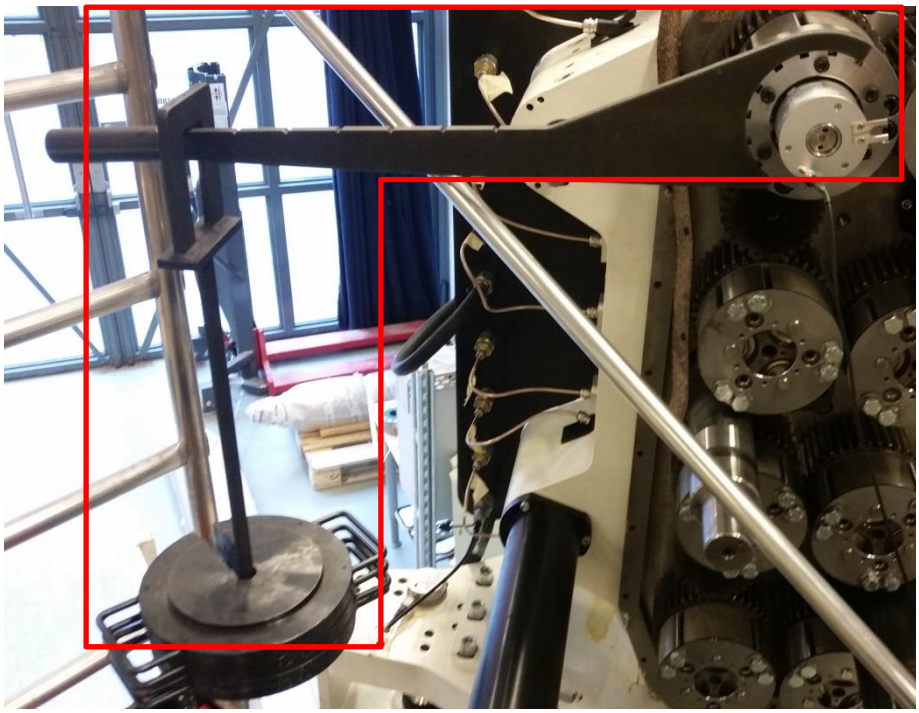

Figure 5. To simulate a load on the flex mechanisms an arm with calibrated weights were used.

To verify the results from the manual stiffness measurements the total relative displacement of all flex units and the rack force during the static test of the load sharing were used. Averaging the results from all flex units generated a mean stiffness curve. The mean stiffness curve of the flex unit measurements was then compared with the mean stiffness curve from the static load sharing tests, see Figure 6.

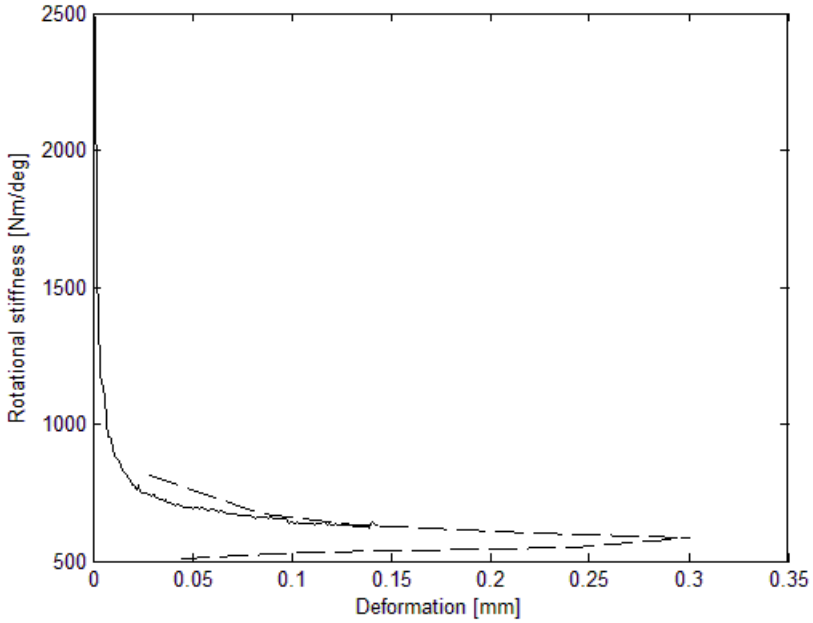

Figure 6. The mean stiffness curve from the manual stiffness measurements of the flex units compared to the static test mean stiffness curve.

By the use of *MATLABs* "Basic Fitting" a general mean stiffness expression could be obtained. Based on the overall mean stiffness of all flex units and each respective flex units mean stiffness a stiffness ratio for each flex unit was assigned. The mean stiffness expression was then multiplied with the stiffness ratios to obtain each flex units individual stiffness curve.

3.3 Load sharing measurements

In order to get a good idea of the actual load sharing behaviour of the Cascade gearbox and allow proper calibration of the models both static and dynamic measurements where conducted on the test rig. The static measurements where done by locking the output shaft of the gearbox with a disc brake. This made it possible to apply force to the rack and measure the load sharing in conditions resembling static. The dynamic measurements where conducted by running the test rig in a regular fashion. Both test setups were executed under varying as well as constant loads of different magnitude.

To evaluate the performance of the Cascade gearbox the load sharing values had to be extrapolated to achieve approximated values of the load sharing during higher loads then during the measurements. Since the stiffness of the flex units is assumed to be linear after the initial deformation the absolute offset from the ideal load would remain the same during the entire linear stiffness deformation. With this assumption it is possible to approximate the load sharing during higher loads then during the physical measurements.

A simple frequency analysis were conducted in order to evaluate were the oscillations in the input rack load originated with the help of the *MATLAB* command *fft()* which provides the frequency spectrum for the input vector.

3.4 Static model

The static model of the cascade gearbox is primarily based on classical gear mechanics. However since the system is overdetermined, i.e. the contact condition between gears are unknown, the model is simulating the Cascade gearbox in small steps to allow analysis of every gear contact in every step. The model is built up by programming logic with a large number of for- and if-conditions in *MATLAB* regulating how much each gear moves. Twist of the flex units start once every gear is in contact from that specific pinion to the output gear. The force ideally transferred from the rack to the pinion gears without any losses is proportional to the twist in the flex mechanisms and is defined as

$$F_{p,i} = \frac{k_i^{\theta} \cdot \theta_i}{d_p/2} \qquad [N] \tag{6}$$

and the total force transferred by all pinions is defined as

$$F_{p,tot} = \sum_{i=1}^{n} F_{p,i} \qquad [N] \tag{7}$$

where k_i^{θ} is the rotational stiffness in the flex mechanisms, n the number of pinions, θ_i is the twist in each flex mechanism and d_p is the diameter of the pinion gears. No more twist is introduced once the total force transferred by all pinions is equal to or larger than the force of the rack. The dimensionless load sharing factor is subsequently defined as

$$LS_{p,\mathrm{i}} = \frac{F_{p,\mathrm{i}}}{F_{p,tot}}. \tag{8}$$

3.5 Dynamic model

A nonlinear time-varying model was used to simulate the gearbox's dynamic behavior. It is based on differential equations accounting for the varying gear mesh stiffness depending on the momentary number of teeth in contact as well as varying tolerance errors, stiffness of the flex mechanisms and whether or not contact between gears are present. The resemblance of a planetary gear is taken advantage of in order to implement an existing model which only necessitates minor modifications to give an accurate representation of the Cascade gearbox where each gear interaction described as Figure 7 and arranged as described in Figure 3.

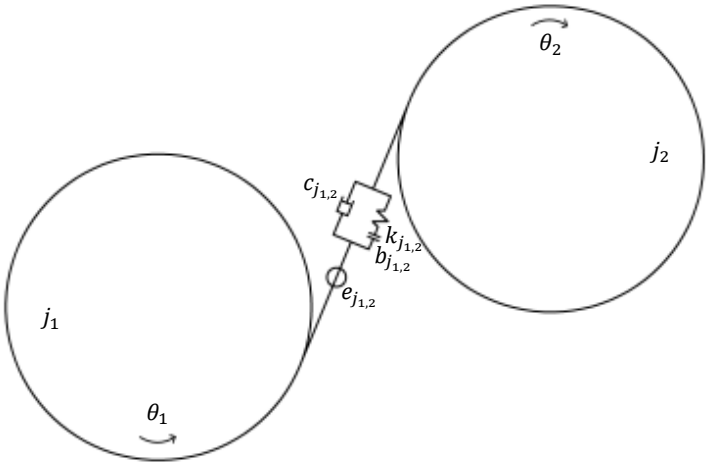

Figure 7. Model of gear pair interaction.

In order to give better understanding and simplify the modelling of the Cascade gearbox it is possible to describe the system as a translational mass-spring-damper system, see Figure 8.

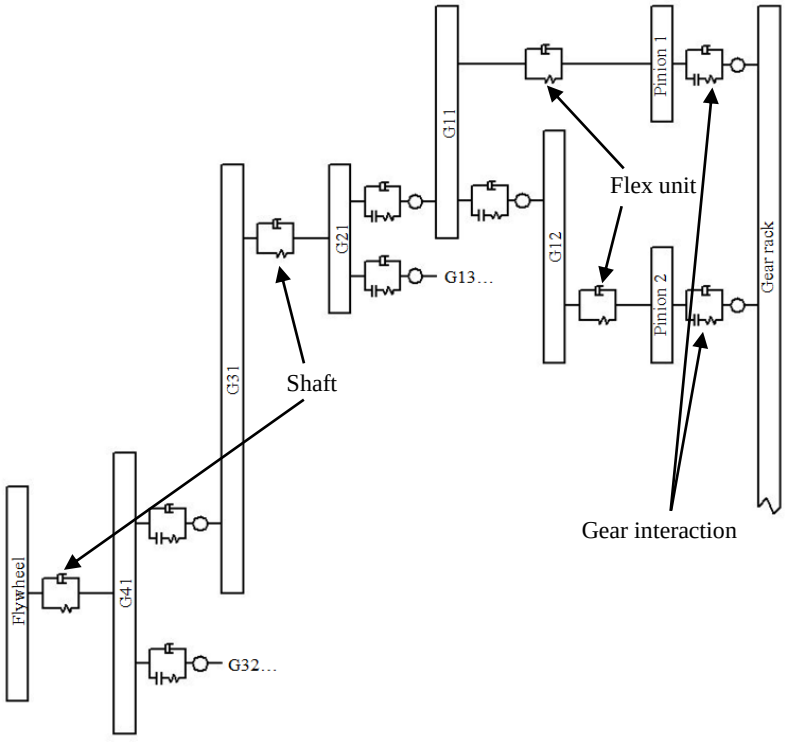

Figure 8. Simplified translational gearbox model from rack to flywheel for two pinions.

Model formulation

The model is restricted to rotational motion only resulting in a 23 DOF model with 18 gear and 11 shaft interactions. The translational equations of motion for a gear pair consisting of the driving gear-j_1 and the driven gear-j_2 in general forms are defined according to (Peng and Wu, 2014) and (Kahraman, 1994a) as

$$m_j \ddot{p}_{j_{1,2}} + h_{j_{1,2}} c_{j_{1,2}} \dot{p}_{j_{1,2}} + h_{j_{1,2}} k_{j_{1,2}}(t) g\left(p_{j_{1,2}}\right) = f_{m,j_{1,2}}(t) + f_{a,j_{1,2}}(t) \tag{9}$$

where m_j is the mass, $k_{j_{1,2}}$ and $c_{j_{1,2}}$ are gear mesh stiffness and damping respectively. $h_{j_{1,2}}$ represents a discontinuous step function approximated with the *MATLAB* function *smf()* which gives an S-shaped curve for improved performance of the *MATLAB* ode-solver defined as

$$h_{j_{1,2}}(g) = smf\left(g\left(p_{j_{1,2}}\right), \left[0 \;\; 1\cdot 10^{-10}\right]\right) \tag{10}$$

where the values specified inside the hard brackets are the extremes in the slope and $g\left(p_{j_{1,2}}\right)$ is the piecewise relative gear mesh displacement function modelled according to (Kahraman, 1994a), (Rao et al., 2014) and (Chen and Wu, 2009) which incorporates the backlash defined as

$$p_{j_{1,2}}(t) = \frac{\left(q_{j1} x_{j_1} - q_{j_2} x_{j_2}\right)}{q_{j_3}} + e_{j_{1,2}}(t) \tag{11}$$

$$g(p_{j_{1,2}}) = \begin{cases} p_{j_{1,2}}(t) - b_{j_{1,2}} & p_{j_{1,2}}(t) > b_{j_{1,2}} \\ 0 & 0 \le p_{j_{1,2}}(t) \le b_{j_{1,2}} \\ -p_{j_{1,2}}(t) & p_{j_{1,2}}(t) < 0 \end{cases} . \tag{12}$$

Here $p_{j_{1,2}}(t)$ is the relative gear mesh displacement, x_{j_n} $n = (1\ to\ 2)$ the translational displacement of driving and driven gear respectively, $q_{j_n} = 1$ for gear interactions and $q_{j_n} = r_{j_n}$ for shaft interactions where r_{j_3} is the radius of the flex unit, $e_{j_{1,2}}(t)$ is the pitch deviation error function and $b_{j_{1,2}}$ the backlash value of each respective gear interaction.

The total system is represented in matrix form according to (Kahraman, 1994a) as,

$$M\ddot{X} + C(t)\dot{X} + K(t)X = F_m(t) + F_a(t) . \tag{13}$$

where M is the diagonal mass matrix, $C(t)$ the damping matrix, $K(t)$ the time varying mesh stiffness matrix, $F_m(t)$ input force vector, see Appendix A: Matrix Representations, $F_a(t)$ the alternating force vector compensating for the error and backlash excitation and X the displacement vector defined as

$$X = \begin{bmatrix} x_r \\ x_{G4} \\ x_{G31} \\ x_{G32} \\ x_{G21} \\ x_{G22} \\ x_{p1} \\ x_{G11} \\ \vdots \\ x_{p8} \\ x_{G18} \\ x_f \end{bmatrix} . \tag{14}$$

The diagonal mass matrix M is defined according to (Kahraman, 1994a) as,

$$M = diag\left[M_r, M_{r2}, M_{G4}, M_{G31}, M_{G32}, M_{G21}, M_{G22}, M_{p1}, M_{G11}, \ldots, M_{p8}, M_{G18}, h_{G4f} \cdot M_f \right] \tag{15}$$

where $M_j = J_j / \left(d_j/2\right)^2$ is the rotational inertia of each gear and h_{G4f} is the discontinues step function determining whether the flywheel should be engaged or not.

The time varying mesh stiffness matrix is given by the equations of motion and builds upon previous work by (Kahraman, 2001), (Lim and Li, 1999) and (Rao et al., 2014) and is defined as

$$K(t) = \begin{bmatrix}
K_r & 0 & 0 & 0 & 0 & 0 & -k^h_{rp1}(t) & 0 & -k^h_{rp2}(t) & 0 & 0 \\
0 & K_o & -k^h_{G314}(t) & -k^h_{G324}(t) & 0 & 0 & 0 & 0 & 0 & 0 & -k^h_{sG4f} \\
0 & -k^h_{G314}(t) & K_{G31} & 0 & -r_{G2} r_{G3} \cdot k_{s2131} & 0 & 0 & 0 & 0 & 0 & 0 \\
0 & -k^h_{G324}(t) & 0 & K_{G32} & 0 & -r_{G2} r_{G3} \cdot k_{s2232} & 0 & 0 & 0 & 0 & 0 \\
0 & 0 & -r_{G2} r_{G3} \cdot k_{s2131} & 0 & K_{G21} & 0 & 0 & -k^h_{G1121}(t) & 0 & 0 & 0 \\
0 & 0 & 0 & -r_{G2} r_{G3} \cdot k_{s2231} & 0 & K_{G22} & 0 & 0 & 0 & 0 & 0 \\
-k^h_{rp1}(t) & 0 & 0 & 0 & 0 & 0 & K_{p1} & -r_p r_{G1} \cdot k_{f1} & 0 & 0 & 0 \\
0 & 0 & 0 & 0 & -k^h_{G1121}(t) & 0 & -r_p r_{G1} \cdot k_{f1} & K_{G11} & 0 & -k^h_{G1211}(t) & 0 \\
-k^h_{rp2}(t) & 0 & 0 & 0 & 0 & 0 & 0 & 0 & K_{p2} & -r_p r_{G1} \cdot k_{f2} & 0 \\
0 & 0 & 0 & 0 & 0 & 0 & 0 & -k^h_{G1211}(t) & -r_p r_{G1} \cdot k_{f2} & K_{G12} & 0 \\
 & & & & & & & & & & \ddots \; 0 \\
0 & -k^h_{sG4f} & 0 & 0 & 0 & 0 & 0 & 0 & 0 & 0 & 0 \; K_f
\end{bmatrix} \tag{16}$$

Where r_j is gear radius, superscript h represents each respective stiffness contact constraint function defined as $h_{j_{1,2}}$ above and K_j represents the combined stiffness of all interactions for that specific gear, for example

$$K_{p1} = h_{rp1} \cdot k_{rp1}(\mathrm{t}) + r_p^2 k_{f1}. \tag{17}$$

The corresponding damping matrix retains the same structure as the stiffness matrix and is found in Appendix A: Matrix Representations.

The alternating force vector compensating for the backlash and error excitation is defined according to (Kahraman, 1994a) as

$$F_a = \begin{bmatrix} -\sum f_{brpn} \\ \sum f_{bG3n4} \\ -f_{bG314} \\ -f_{bG324} \\ \sum f_{bG1n21} \\ \sum f_{bG1n22} \\ f_{brp1} \\ f_{bG1211} - f_{bG1121} \\ f_{brp2} \\ -f_{bG1211} \\ \vdots \\ f_{brp7} \\ f_{bG1817} - f_{bG1722} \\ f_{brp8} \\ -f_{bG1817} \\ 0 \end{bmatrix} + \begin{bmatrix} -\sum f_{erpn} \\ \sum f_{eG3n4} \\ -f_{eG314} \\ -f_{eG324} \\ \sum f_{eG1n21} \\ \sum f_{eG1n22} \\ f_{erp1} \\ f_{eG1211} - f_{eG1121} \\ f_{erp2} \\ -f_{eG1211} \\ \vdots \\ f_{erp7} \\ f_{eG1817} - f_{eG1722} \\ f_{erp8} \\ -f_{eG1817} \\ 0 \end{bmatrix} \tag{18}$$

with components defined as

$$f_{bj_{1,2}} = -h_{j_{1,2}}(g) \cdot \left(b_{j_{1,2}} k_{j_{1,2}} \right), \tag{19}$$

$$f_{ej_{1,2}} = h_{j_{1,2}}(g) \cdot \left(c_{j_{1,2}} \dot{e}_{j_{2,2}}(t) + e_{j_{1,2}}(t) k_{j_{1,2}}(t) \right). \tag{20}$$

The pitch deviation error function simulating the varying error during a full revolution is defined according to (Kahraman, 1994a) as

$$e_{j_{1,2}}(t) = e_{ampj_{1,2}} \cdot \sin\left(\frac{w_{j_{1,2}}(t) \cdot t}{Z_{j_2}} + \varepsilon_{j_2} + \psi_{j_2} \right) \tag{21}$$

where $e_{ampj_{1,2}}$ is the amplitude of the pitch deviation error, $w_{j_{1,2}}$ is the gear mesh frequency, Z_{j_2} the number of gear teeth in the driven gear, ψ_{j_2} the position angle of the driven gear (Kahraman, 1994b) and ε_{j_2} the position of the gear pitch deviation error according to (Kahraman, 1994a).

Similarly the varying stiffness function is defined also according to (Kahraman, 1994a) as

$$k_{j_{1,2}}(t) = k_{ampj_{1,2}} \cdot \left[1 + k_{mult} \cdot \sin\left(w_{j_{1,2}}(t) \cdot t + Z_{j_2} \cdot \psi_{j_2} + \varphi_{j_2} \right) \right] \tag{22}$$

where k_{amp} is the average stiffness, k_{mult} the dimensionless constant governing the maximum number of gears teeth in contact at any one time and φ_{j_2} the phase angle according to (Kahraman, 1994b).

Since the aim of the model is to simulate the load sharing characteristics between the pinions with the present flex mechanism it is logical to calculate the load sharing at these points. Also important is the transmitted force in each flex unit defined as

$$F_{j_{1,2}} = h_{j_{1,2}} \cdot c_{j_{1,2}} \cdot \dot{p}_{j_{1,2}} + h_{j_{1,2}} \cdot k_{j_{1,2}}(t) \cdot g(p_{j_{1,2}}). \tag{23}$$

The load sharing factor is then obtained as the quotient of the transmitted force in one flex unit and its ideal counterpart defined as

$$LS_{rpn} = \frac{F_{rpn}}{\sum F_{rpn}}. \tag{24}$$

A load sharing factor of 1/8 indicates a perfect load sharing, meaning that the transmitted force perfectly correspond with the ideal. A load sharing factor smaller than 1/8 indicates that the transmitted force is smaller than the ideal. In the same way does a load sharing factor larger than 1/8 indicate a transmitted force larger than the ideal.

Solution

The nonlinear time-varying model is solved with numerical integration in *MATLAB's* built in ordinary differential equation solver, from here on known as ode-solver. Since the ode exhibits a stiff behavior *ode15s* is used. It is specifically adapted for stiff ode's and is a variable order multi step solver based on the numerical differentiation formulas (Ashino et al., 2000).

Frequency analysis

The natural frequencies of the gearbox were analyzed using the eigenvalue problem of the undamped system including only the stiffness and mass matrices, defined according to (Lallement and Inman, 1995) as

$$(-M\omega^2 + K)u = 0. \tag{25}$$

By solving the eigenvalue problem with *MATLAB's* built in function *eig()* it is possible to get the eigenvalues and eigenvectors of the system. Taking the square root of the eigenvalues then gives the natural frequencies, (Lallement and Inman, 1995). During these calculations stiffness and contact constraints were constant.

4 RESULTS

In this chapter results from both models along with results from the physical measurements are presented and compared.

4.1 Tolerance analysis

The tolerance analysis resulted in pitch deviation distributions for each gear interaction. Most vital to the load sharing is the error distribution between the rack and pinion, see Figure 9. Pitch deviation distributions for the other gear interactions is found in Appendix B: Additional Figures. The largest error deviation for these gears was *±70 µm*. The overall largest error deviation is *±0.1 mm* in the G1 to G1 interactions.

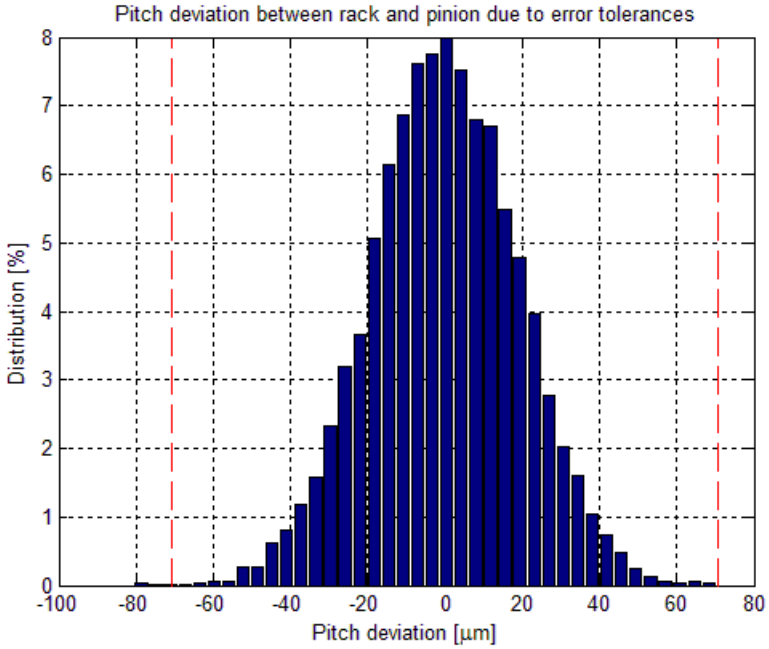

Figure 9. Pitch deviation distribution between for the rack/pinion interaction.

The tolerance with the largest effect on the tolerance chain affecting the rack/pinion interaction is the pitch deviation of the rack followed by the pitch deviation caused by the rack runout, see Table 2. For the other gear interactions positional errors of the shaft had the biggest effect as found from Spearman's rank coefficient. This indicates that these are the tolerances most effort should be devoted to initially for maximum effect.

Table 2. Tolerances and their effect on the tolerance chain for the rack/pinion interaction expressed with Spearman's rank coefficient.

Tolerance	Rank
Pitch deviation pinion	0,34973
Runout pinion	0,10857
Pitch deviation rack	0,78369
Runout rack	0,38744
Pinion position xy	0,18094
Pinion axle angle	0,10194

4.2 Stiffness measurement

Results from the manual measurements of the flex unit stiffness showed a higher stiffness then the *430 Nm/deg* specified by the supplier. This was evident in both the manual stiffness tests as well as in the static load sharing measurements, for pinion 1 see Figure 10. Stiffness comparisons for the remaining pinions are available in Appendix B: Additional Figures.

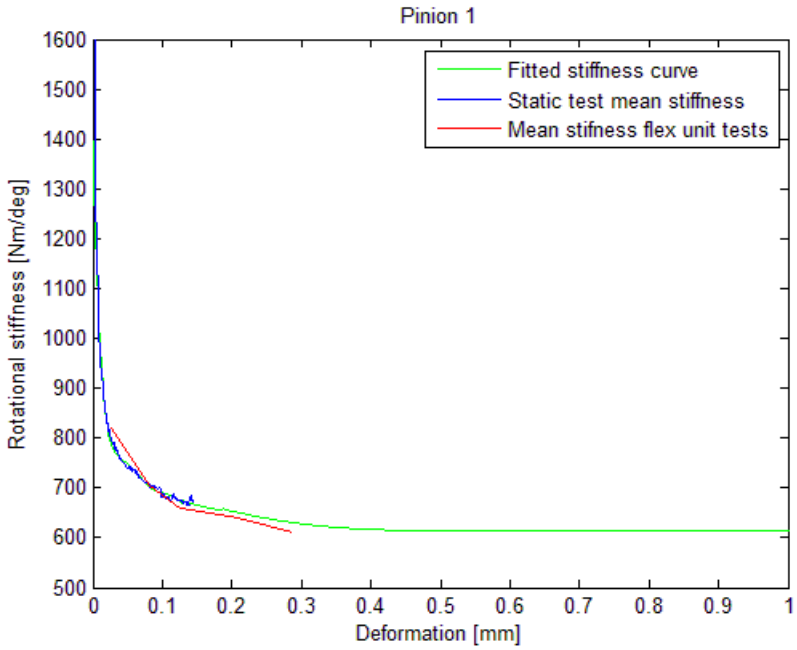

Figure 10. Stiffness curves for the manual stiffness measurements (red), static load sharing measurements (black) and the fitted data (blue) for pinion 1.

From the results of the manual stiffness measurements and the static load sharing measurements a fitted stiffness curve was approximated using *MATLABs "Basic fitting"*. The equation for the approximated rotational stiffness is defined as

$$k_{fi}^{\theta} = H_{d,1}(3{,}6123\cdot10^{27}\cdot p_{fi}^{\ 6} - 1{,}8123\cdot10^{24}\cdot p_{fi}^{\ 5} + 3{,}6137\cdot10^{20}\cdot p_{fi}^{\ 4} - 3{,}6392\cdot10^{16}\cdot p_{fi}^{\ 3} + 1{,}943\cdot10^{12}\cdot p_{fi}^{\ 2}$$
$$-5{,}3249\cdot10^{7}\cdot p_{fi} + 1306{,}7) + H_{d,2}(1{,}5651\cdot10^{17}\cdot p_{fi}^{\ 4} - 1{,}3323\cdot10^{14}\cdot p_{fi}^{\ 3} + 4{,}1715\cdot10^{10}\cdot p_{fi}^{\ 2}$$
$$-5{,}9716\cdot10^{6}\cdot p_{fi} + 950{,}51) + H_{d,3}\cdot(6{,}716\cdot10^{8}\cdot p_{fi}^{\ 2} - 5{,}7413\cdot10^{5}\cdot p_{fi} + 699{,}8) + H_{d,4}\cdot 575$$

where p_{fi} is the relative flex deformation in the flex unit and $H_{d,n}$ $(n = 1\ to\ 4)$ is Heaviside's function defined as

$$H_{d,1} = \begin{cases} H_{d,1} = 1, & p_{fi} \le 0,00013 \\ H_{d,1} = 0, & p_{fi} > 0,00013 \end{cases}, \tag{26}$$

$$H_{d,2} = \begin{cases} H_{d,2} = 1, & 0,00013 < p_{fi} \le 0,000187 \\ H_{d,2} = 0, & 0,00013 > p_{fi} > 0,000187 \end{cases}, \tag{27}$$

$$H_{d,3} = \begin{cases} H_{d,3} = 1, & 0,000187 < p_{fi} \le 0,00042 \\ H_{d,3} = 0, & 0,000187 > p_{fi} > 0,00042 \end{cases}, \tag{28}$$

$$H_{d,4} = \begin{cases} H_{d,4} = 1, & p_{fi} > 0,00042 \\ H_{d,4} = 0, & p_{fi} < 0,00042 \end{cases}. \tag{29}$$

When the deformation is larger than *0,00042m (0,42mm)* the stiffness becomes linear with an average spring stiffness of *575 Nm/deg*. This stiffness is the mean for all pinions and is assumed to be constant during the rest of the deformation, see Figure 11.

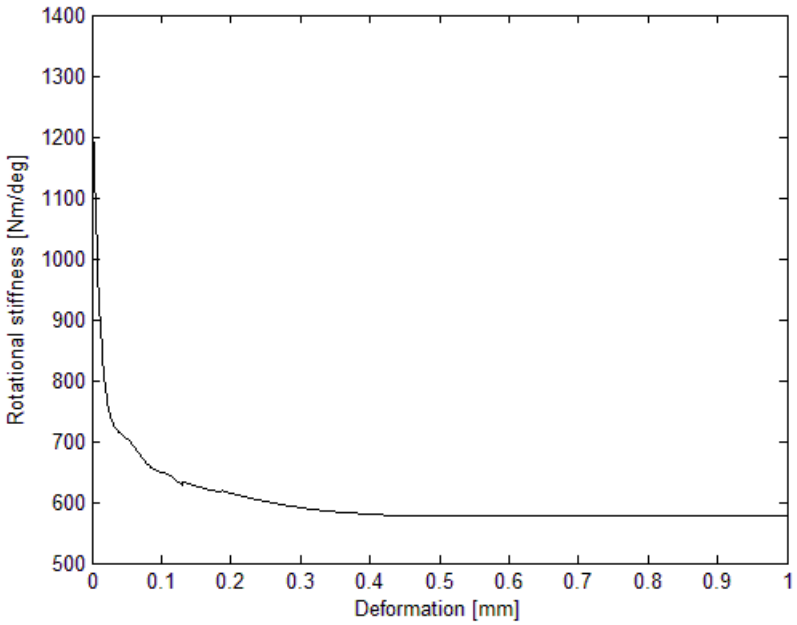

Figure 11. The fitted mean stiffness curve plotted against the deformation.

The stiffness measurements derived from the mean stiffness of the results from the manual stiffness measurements and the mean stiffness from each flex unit displayed an overall spread of *15,8%* (*-7,3% to +8,5%*), see Table 3. This could be compared to the supplier specified *±20%* stiffness deviation.

Table 3. Stiffness ratios derived from the overall mean stiffness and each flex unit's respective mean stiffness.

Pinion	Ratio [-]
1	1,06831672
2	1,01555172
3	0,9765572
4	1,08467615
5	0,95981637
6	0,96769169
7	1,04315065
8	0,92739015

4.3 Load sharing measurements

Both the dynamic test results as well as the static ones exhibited the same load sharing characteristics regardless of load condition. During very low loads the load sharing was poor, especially in direction $\vec{B}$. However when loaded more heavily load sharing improved significantly in both directions even though direction $\vec{A}$ still displayed smaller differences and better overall performance.

Static

The results from the static measurements were, due to its nice behavior, used to verify the manual stiffness measurements, serve as data for the fitted stiffness curve, verify the static and dynamic models as well as to initially identify specific characteristics of the Cascade gearbox. A characteristic behavior of the Cascade gearbox identified from the static measurements was the negative effect the deliberate geometrical differences had on the load sharing performance. These geometric differences caused the even numbered pinions to carry a smaller load initially, see Figure 12. This previously unknown behavior causes the Cascade gearbox to apply a lateral force on the gear rack.

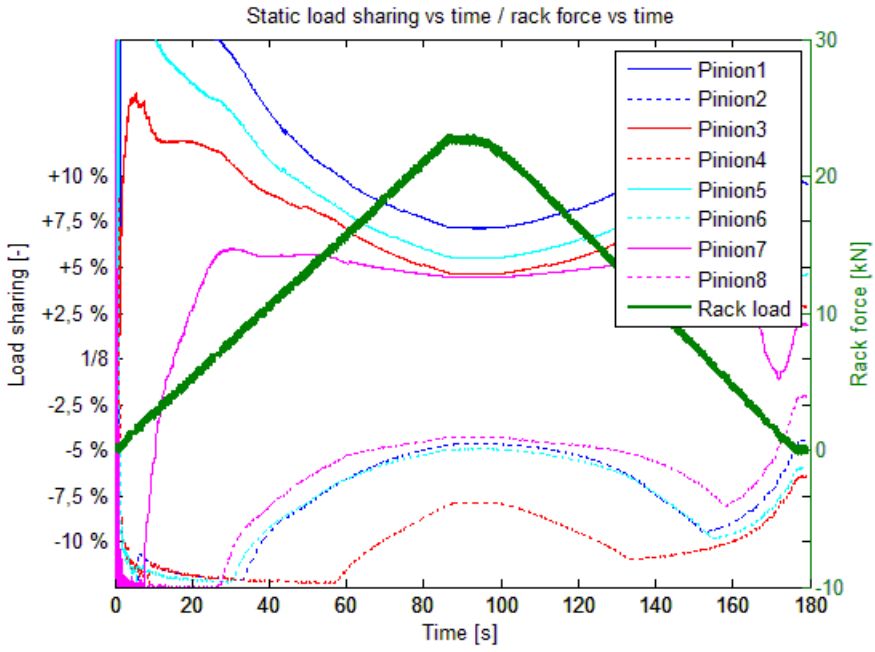

Figure 12. The static load sharing together with the rack force plotted against time. The even pinions do not take any load in the beginning due to the geometric differences.

However this behaviour was only registered when applying load in direction $\vec{B}$. This is due to the geometric differences not having any effect on the load sharing in direction $\vec{A}$, see Figure 13.

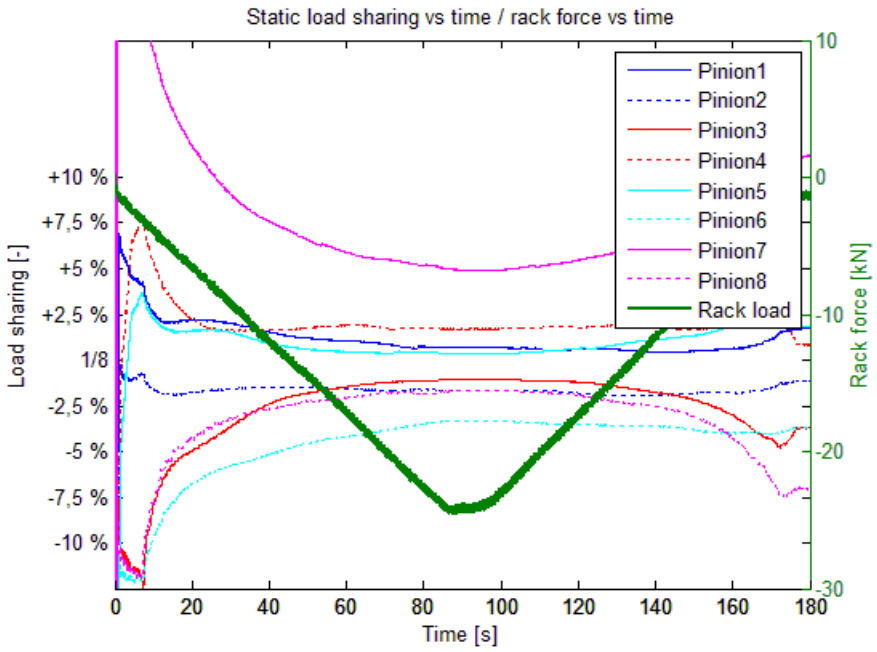

Figure 13. The static load sharing together with the rack force plotted against time. The pinions all take part of the load from the beginning. This is due to the geometric differences not having any effect in direction $\vec{A}$.

Since the maximum load used in the static measurements is *23 kN* and the gearbox is designed for a maximum load of *247 kN* approximations for the load sharing during higher loads had to be made, see Figure 14 and Figure 15.

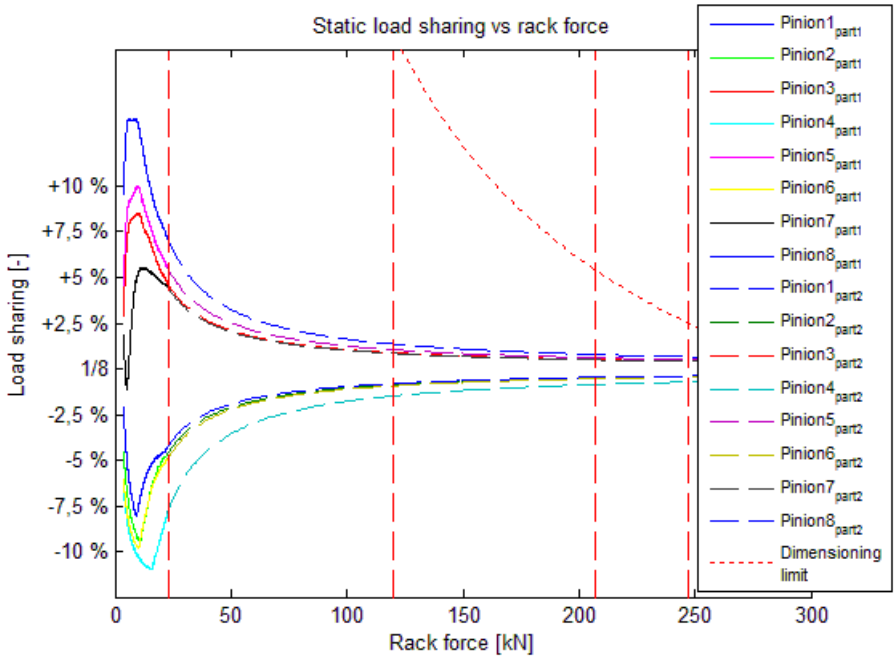

Figure 14. Extrapolated static load sharing and the dimensioning limit plotted against rack force in direction $\vec{B}$. The vertical dashed lines mark loads of *23*, *120*, *207* and *247 kN* respectively.

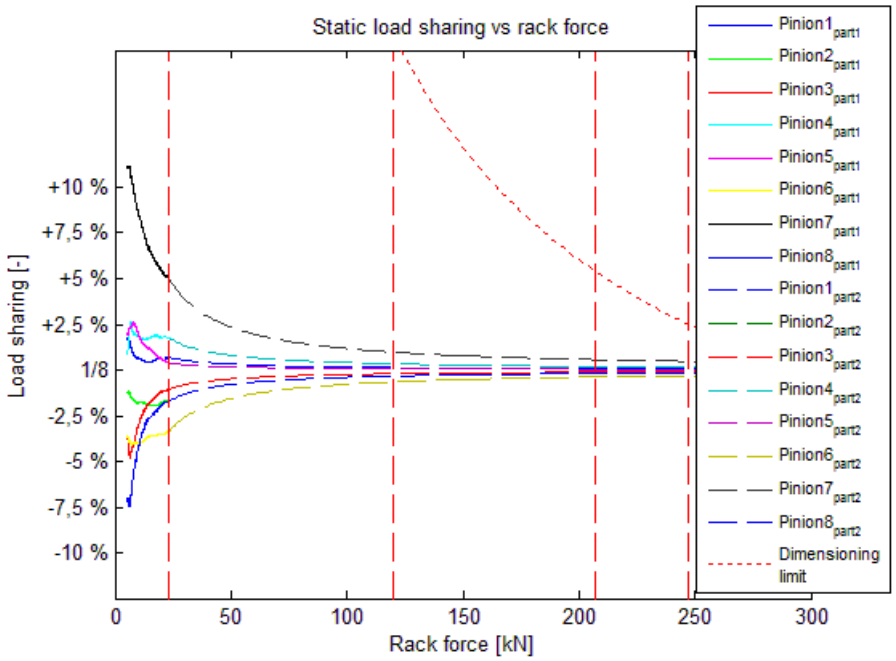

Figure 15. Extrapolated static load sharing and the dimensioning limit plotted against rack force in direction $\vec{A}$. The vertical dashed lines mark loads of *23, 120, 207* and *247 kN* respectively.

Assuming constant load differentiation and linear and equal flex unit stiffness above *23 kN* approximated values for the load sharing could be calculated, see Table 4. These results demonstrates that no pinion take more than *0,6%* overload during maximum load conditions which is less than the *2,5%* the gears are dimensioned for.

Table 4. Measured load sharing factor at *23 kN* and approximated values for *120*, *207* and *247 kN* in direction $\vec{B}$ assuming linear stiffness and constant load differentiation after *23 kN*. Perfect load sharing is 1/8=0.125.

Pinion	23 kN	120 kN	207 kN	247 kN
1	0,195418	0,138541	0,132841	0,131569
2	0,078937	0,116146	0,119873	0,120704
3	0,170688	0,133782	0,130085	0,12926
4	0,047478	0,11001	0,116372	0,117771
5	0,179358	0,135448	0,13105	0,130069
6	0,076231	0,115626	0,119572	0,120453
7	0,168922	0,133442	0,129888	0,129095
8	0,082933	0,116914	0,120318	0,121077
Mean LS uneven	0,1785965	0,1353033	0,130966	0,1299983
Mean LS even	0,0713948	0,114674	0,119034	0,1200013

Noticed was that the load sharing behavior differs substantionally between direction $\vec{A}$ and direction $\vec{B}$. In direction $\vec{B}$ it is apparent that the uneven pinions initally take no load and then start to take load as the total load increases which reduce the effect of the geometric differences. Results from direction $\vec{A}$ however show a much smoother load sharing where there is a mix of even and uneven pinions taking more than the ideal 1/8 of the total load. As a result, the load sharing is much better even at higher loads since the load differentiation is smaller when the flex unit stiffness enters its linear phase.

Dynamic

The results from the dynamic measurements showed a much more chaotic behavior then the static results. This is due to the rapid changes between high load and low load. However despite this the same load sharing behavior could be distinguished when loaded. It is evident that the performance is highly dependent on the load since peaks of the load sharing factor indicate overload well above *10%* during low loads, see Figure 16. This is however no problem since the load sharing factor is a relative value. The absolute load on each pinion is, during these conditions, nowhere near its dimensioning limit.

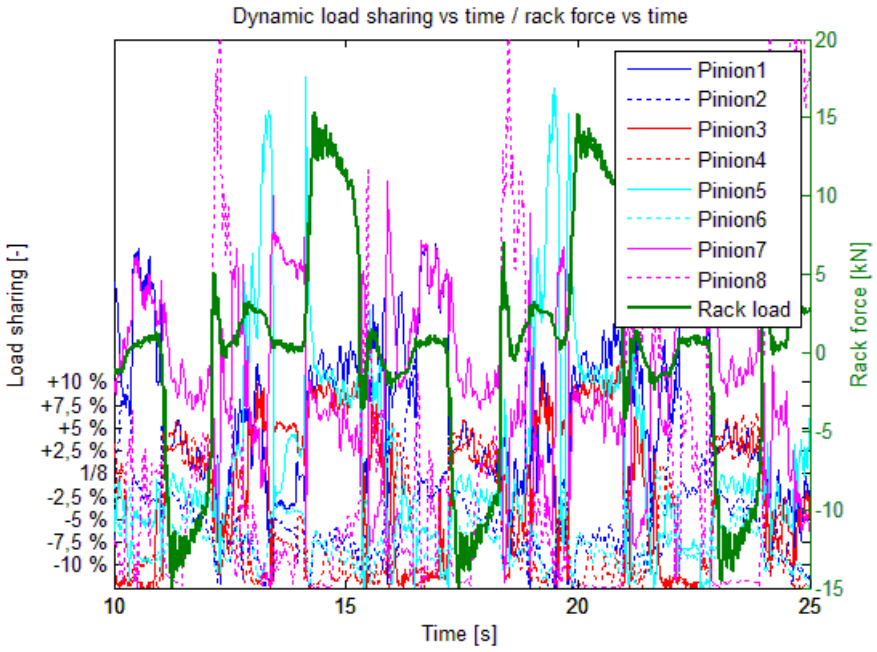

Figure 16. Load sharing results from the dynamic measurements over two full periods plotted against time together with the rack load.

Zooming in to just half a period showing the dynamic behavior during one load cycle it is possible to analyze the load sharing behavior in direction $\vec{B}$ and $\vec{A}$, see Figure 17 and Figure 18 respectively.

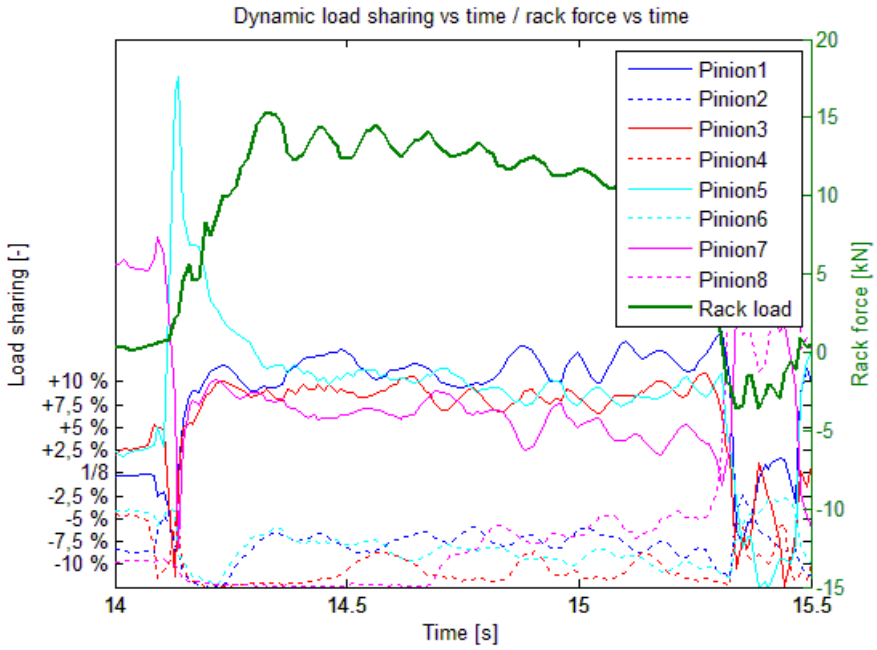

Figure 17. Load sharing results from the dynamic measurements in direction $\vec{B}$ plotted against time together with the rack load.

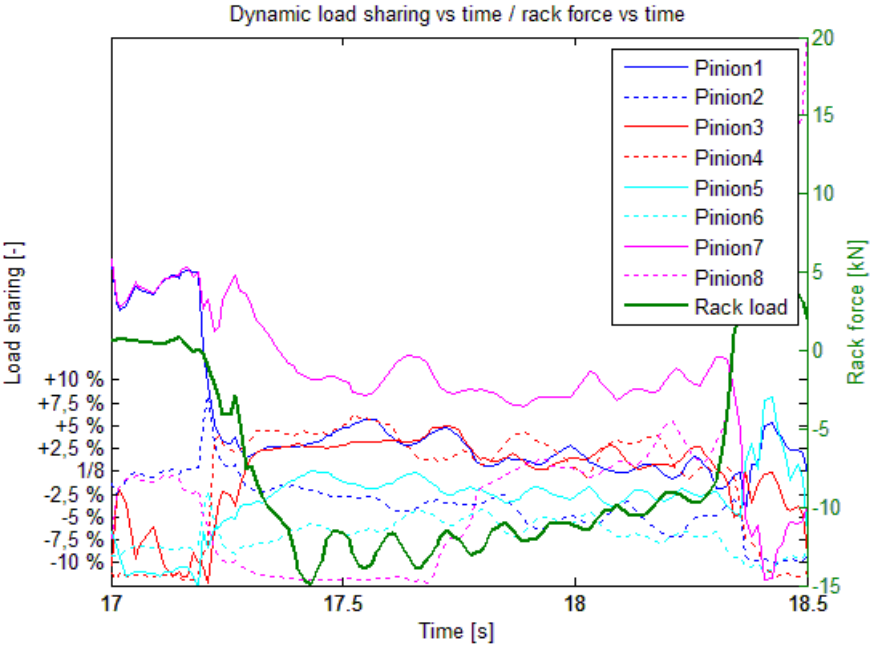

Figure 18. Load sharing results from the dynamic measurements in direction $\vec{A}$ plotted against time together with the rack load.

For the dynamic measurements the maximum rack load reached *14 kN* meaning the same assumptions as for the static measurements had to be made in order to approximate the load sharing during higher loads, see Figure 19 and Figure 20.

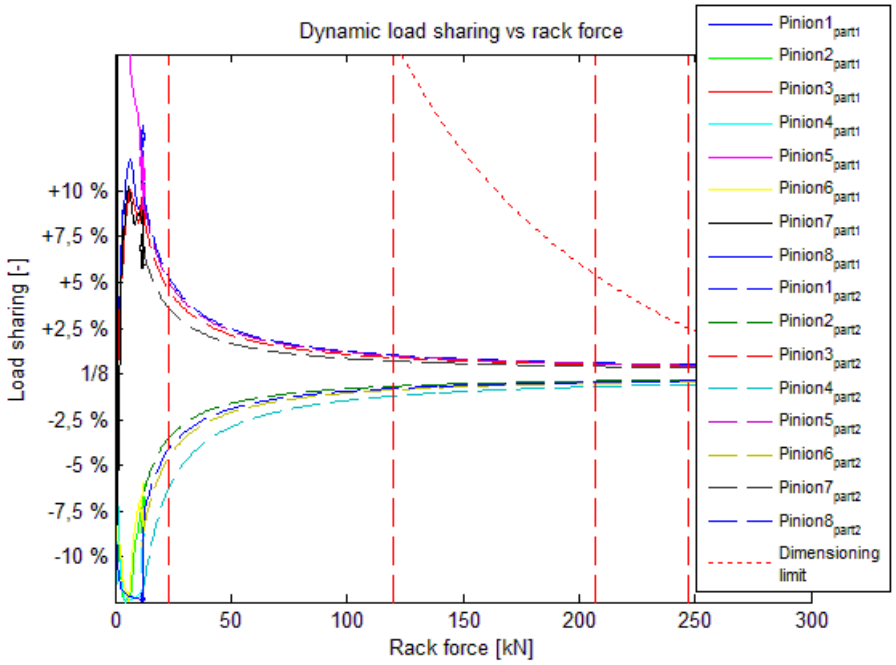

Figure 19. Extrapolated load sharing plotted against rack force in direction $\vec{B}$. No mixing between the uneven and even pinions occurs. The vertical dashed lines mark loads of *23*, *120*, *207* and *247 kN* respectively.

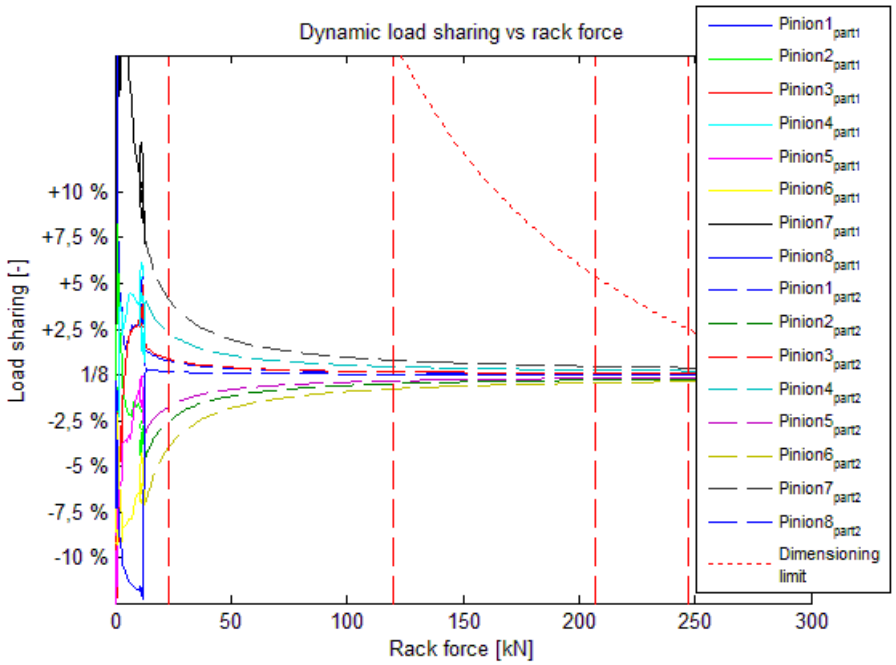

Figure 20. Extrapolated load sharing plotted against rack force in direction $\vec{A}$. Mixing between the uneven and even pinions occur. The vertical dashed lines mark loads of *23*, *120*, *207* and *247 kN* respectively.

The approximated dynamic load sharing results corresponded well with that of the static with a maximum overload of *0,5%* at *247 kN*, again below the dimensioning limit of *2,5%* overload, see Table 5.

Table 5. Measured load sharing factor at *14 kN* and approximated values for *120*, *207* and *247 kN* both in direction $\vec{B}$ assuming linear stiffness and constant load differentiation after *14 kN*. Perfect load sharing is 1/8=0.125.

	Dynamic $\vec{B}$ direction			
Pinion	14 kN	120 kN	207 kN	247 kN
1	0,224558	0,135668	0,131181	0,130118
2	0,055638	0,117567	0,120694	0,122391
3	0,203061	0,133365	0,129847	0,129061
4	0,008211	0,112485	0,117749	0,118924
5	0,217238	0,134884	0,130727	0,129799
6	0,042249	0,116133	0,119862	0,120695
7	0,192549	0,132238	0,129194	0,128914
8	0,056494	0,117659	0,120748	0,121436
Mean LS 1,3,5,7	0,2093515	0,13403875	0,13023725	0,129473
Mean LS 2,4,6,8	0,040648	0,115961	0,11976325	0,1208615

Limiting load

The supplier of the flex units specify a maximum load of *36* kN per flex unit and a maximum deformation of *10%* to achieve good lifetime. This translates to a maximum load of *288 kN* for the entire Cascade gearbox. The *10%* deformation limit gives dimensioning loads as specified by Table 6.

Table 6. Maximum possible loads theoretically without geometrical differences and constant flex unit stiffness, from measurements in direction $\vec{B}$ and $\vec{A}$ where loads higher then achieved during testing is extrapolated the same way as earlier with constant stiffness above *23 kN*.

	Theoretical with no geometrical differences and constant flex unit stiffness							
Pinion	1	2	3	4	5	6	7	8
Max load per pinion [kN]	29,772	28,302	27,0215	30,228	26,749	26,968	29,071	25,845
Max total load [kN]	224,15							
	Extrapolated from measurements direction $\vec{B}$							
Pinion	1	2	3	4	5	6	7	8
Max load per pinion [kN]	30,042	31,619	27,470	32,122	26,987	30,169	29,331	29,355
Max total load [kN]	237,1							
	Extrapolated from measurements direction $\vec{A}$							
Pinion	1	2	3	4	5	6	7	8
Max load per pinion [kN]	35,746	28,545	32,403	30,497	32,598	27,211	37,057	26,075
Max total load [kN]	250,13							

Frequency analysis

The input rack load displayed an oscillating behavior, as seen above in Figure 16, with sampling period determined manually to around *0,122 s*. In the frequency analysis of the input rack load, the peaks at low frequencies correspond with that of the input force period. The frequency response then decreases with higher frequencies apart from a small area around *8 Hz* corresponding with the sampling period of the oscillations, see Figure 21.

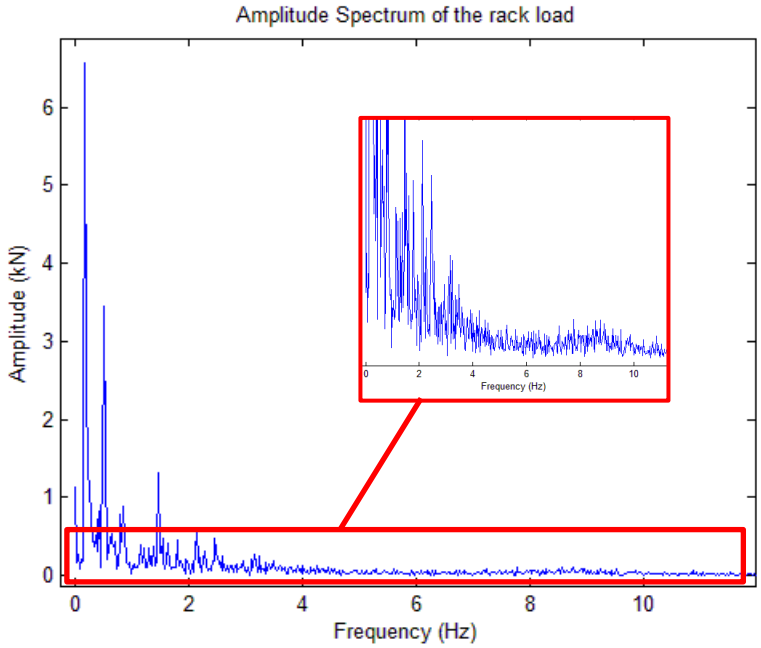

Figure 21. Amplitude spectrum of the input rack load. The highest peaks at low frequencies correspond to the period of the rack movement. The higher frequency response around *8 Hz* corresponds to the noise of the input load.

4.4 Static model

The load sharing of the static model shows the same overall behavior as the measurements indicating a good accuracy. However something the measurements did not pick up that was evident from the results of the static model was the intersection of the load sharing curves from different pinions during higher loads in direction $\vec{B}$, see Figure 22. This is due to the fact that no differences apart from the stiffness ratios acquired from the manual stiffness measurements and the geometric differences exist between the pinions. Since some of the flex units are stiffer they will after all pinions are in contact strive to take more load then others. When the load is increased and the deformation in the flex unit grows they will have the ability to do just that. This theory is given evidence by the fact that the three pinions taking the highest load during high forces are the three pinions corresponding with the highest stiffness. The first crossing of the load sharing curves occurs at *152 kN*.

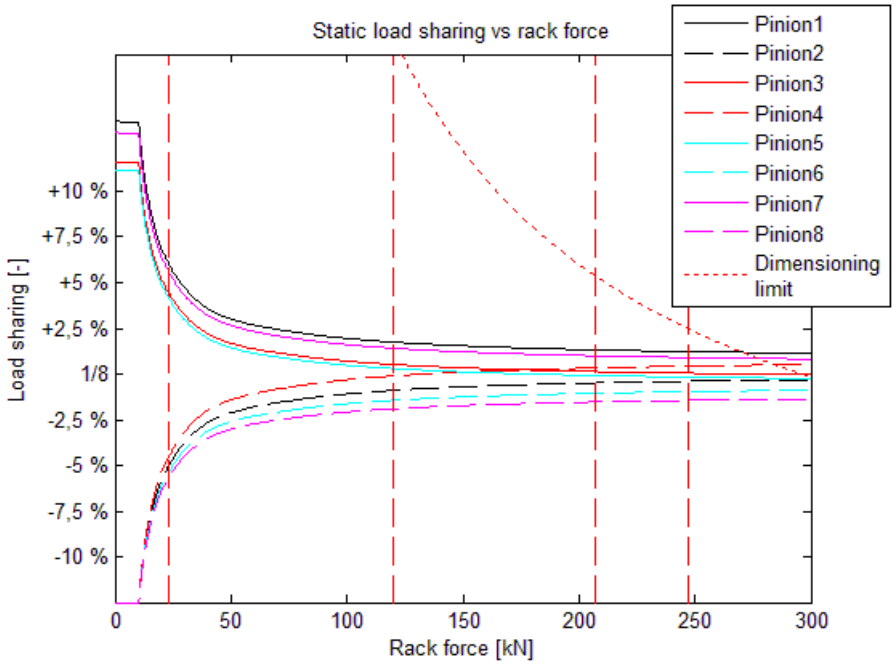

Figure 22. Load sharing results from static model plotted against rack force. The load sharing curves are crossing due to different stiffness ratios. The vertical dashed lines mark loads of *23, 120, 207* and *247 kN* respectively.

With the stiffness ratios removed, crossing of load sharing curves is non-existent, see Figure 23. Differences between the even and uneven pinons do however still occur as a result of the geometric differences in direction $\vec{B}$.

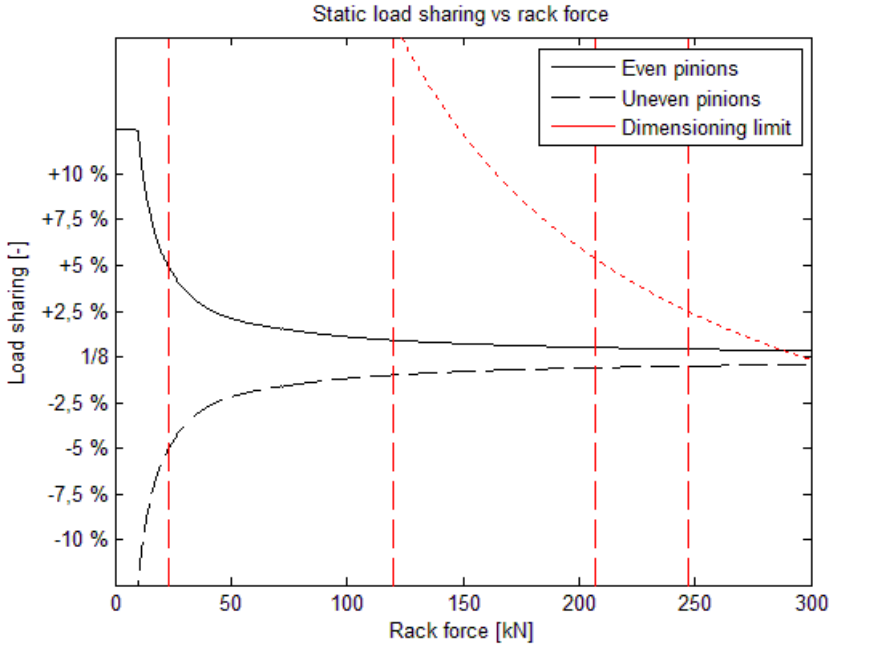

Figure 23. Load sharing results from static model plotted against rack force without stiffness ratios. The even and uneven pinions take exactly the same load within their group due to identical conditions. This removes the crossing of load sharing curves since they all have the same stiffness. The vertical dashed lines mark loads of *23, 120, 207* and *247 kN* respectively.

In direction $\vec{A}$ differences in load sharing is only due to stiffness ratio since there is no geometric differences to upset the balance, see Figure 24. If in addition to that the stiffness ratios are removed a perfect load sharing between the pinions is achieved.

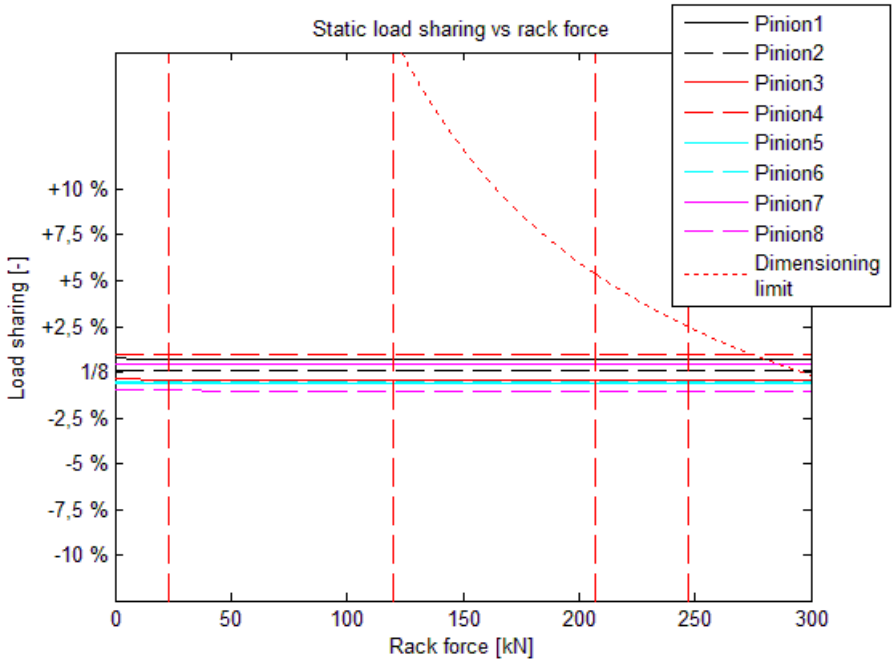

Figure 24. Load sharing results plotted against rack force without geometric difference. Since the conditions between the pinions are identical apart from the stiffness ratios the load sharing remains the same regardless of rack force. The difference is only due to difference in stiffness.

As illustrated above the load sharing behaviour is dependent on direction and load. Results in both directions for *120*, *207* and *247 kN* are presented in Table 7.

Table 7. Load sharing in direction $\vec{B}$ for the static model at *120 kN*, *207 kN*, *247 kN*. Perfect load sharing is 1/8=0.125.

Pinion	120 kN	207 kN	247 kN
1	0,14226	0,13813	0,13721
2	0,11643	0,12041	0,12129
3	0,13004	0,12627	0,12542
4	0,12436	0,1286	0,12955
5	0,12781	0,1241	0,12327
6	0,11095	0,11473	0,11558
7	0,13891	0,13488	0,13398
8	0,10632	0,10996	0,11076
Mean LS 1,3,5,7	0,134755	0,130845	0,12997
Mean LS 2,4,6,8	0,114515	0,118425	0,119295
Mean LS, no stiffness ratio	0,13389	0,13	0,12913
	0,11538	0,11927	0,12013

All results presented from the static model up to this point have been ideal in the sense that no tolerance errors have been included. With errors included the load sharing behaviour is affected with results for a population of 1000 gearboxes as seen in Figure 25 for pinion 1. Results for the remaining seven pinions are found in Appendix B: Additional Figures. Noted is that none of the gearboxes in the population fail due to overload.

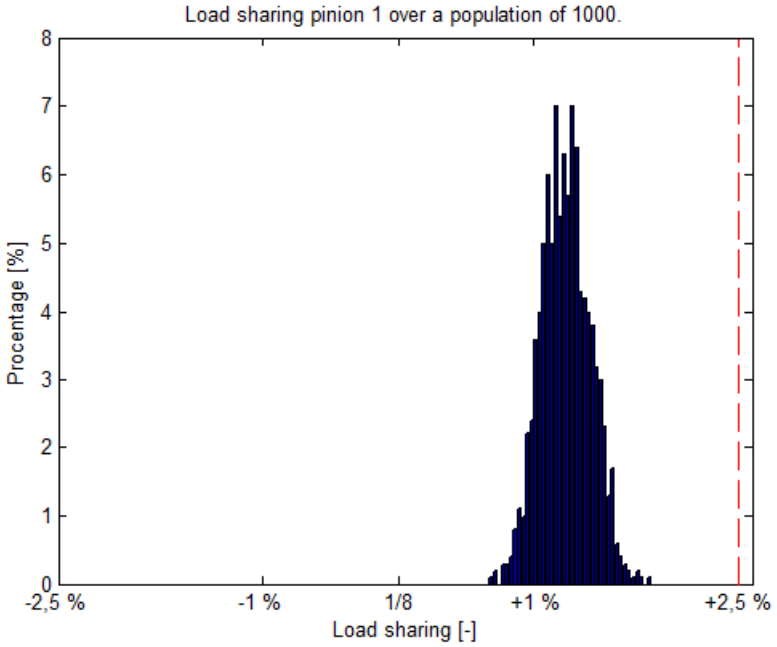

Figure 25. Load sharing at *247 N* for pinion 1 in direction $\vec{B}$ for a population of 1000 gearboxes. None of the gearboxes fail due to overload of more than *2,5%* of the total load above the nominal *1/8*.

4.5 Dynamic model

Results from the dynamic model shared the behavior of the static model and the physical tests with the same unique characteristics visible in the load sharing. The dynamic model gives the added benefit of studying the load sharing during actual movement of the Cascade gearbox with varying mesh stiffness as well as varying errors. This further enhances the understanding of the Cascade gearbox. The chaos during low loads previously identified during the dynamic measurements was however not visible in the same way even though some chaos was present in the results from the dynamic model. This is largely due to a more ideal approach as well as a more stable input load, see Figure 26.

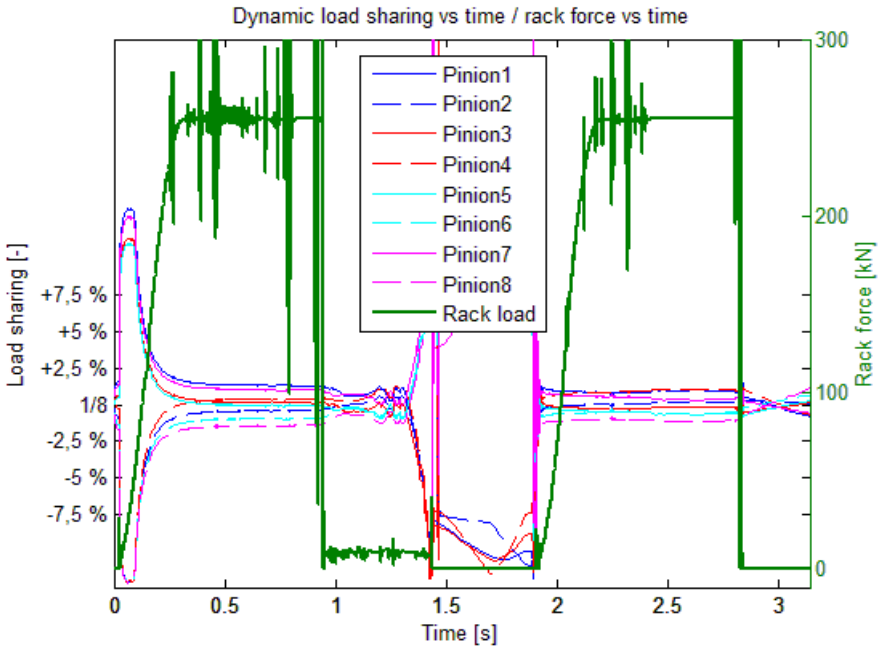

Figure 26. Load sharing for the dynamic model over on complete period. The rack force showed is the absolute, the first peak is in direction $\vec{B}$ and the second in direction $\vec{A}$.

When studying the load sharing characteristics for the dynamic model in one direction the behaviour is more easily distinguished. In direction $\vec{B}$ the same behaviour discovered in the static model is identified. The load sharing curves intersect each other when the initial difference due to the geometrical differences is equal or small compared to the stiffness ratios, see Figure 27.

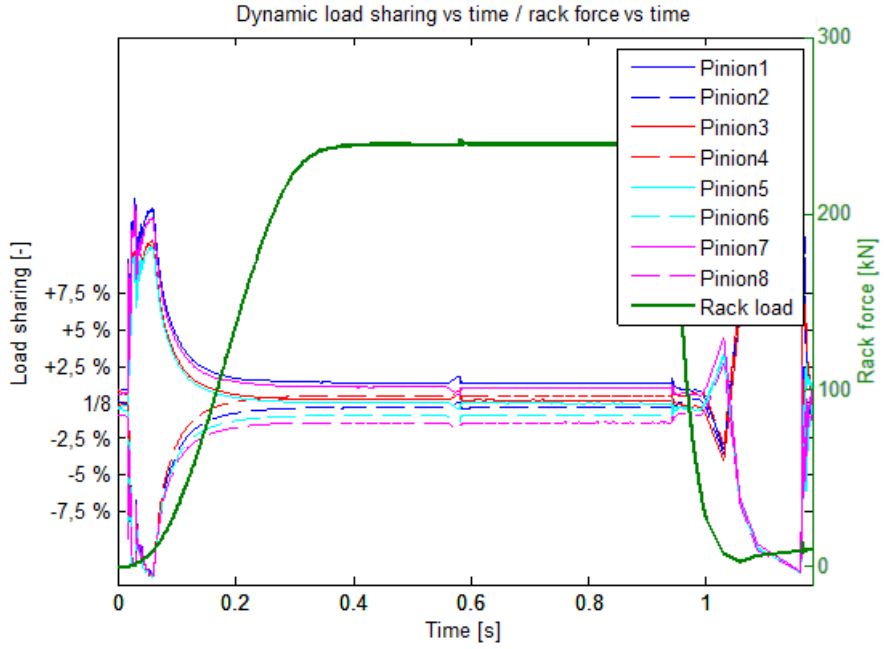

Figure 27. Load sharing for the dynamic model over half a period in direction $\vec{B}$.

In direction $\vec{A}$ load sharing differences are only due to the stiffness ratios, see Figure 28.

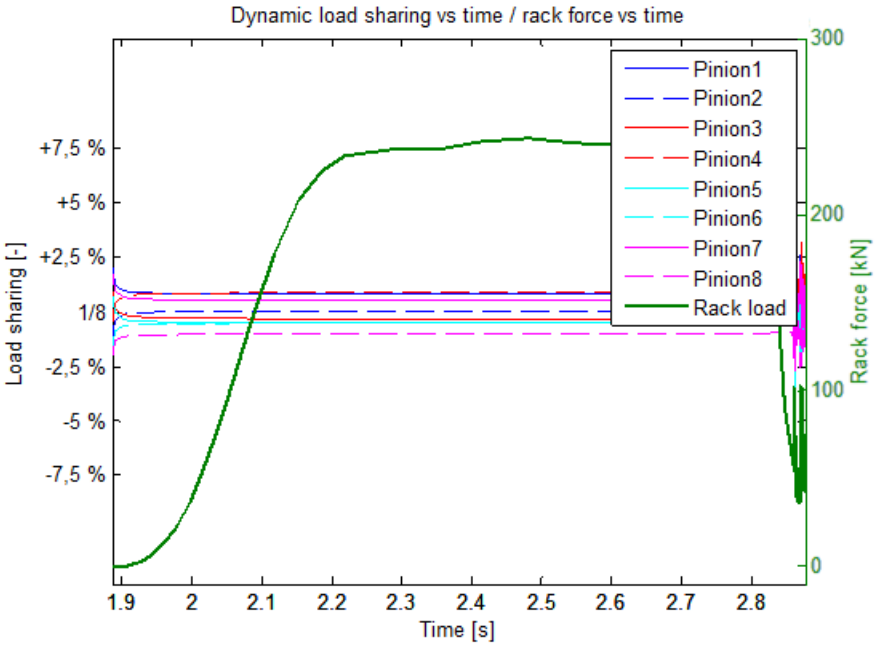

Figure 28. Load sharing for the dynamic model over half a period in direction $\vec{A}$.

The first occurrence of a load sharing curve intersecting another in direction $\vec{B}$ is at *160 kN* when the curve representing pinion 1 crosses that of pinion 5, Figure 29.

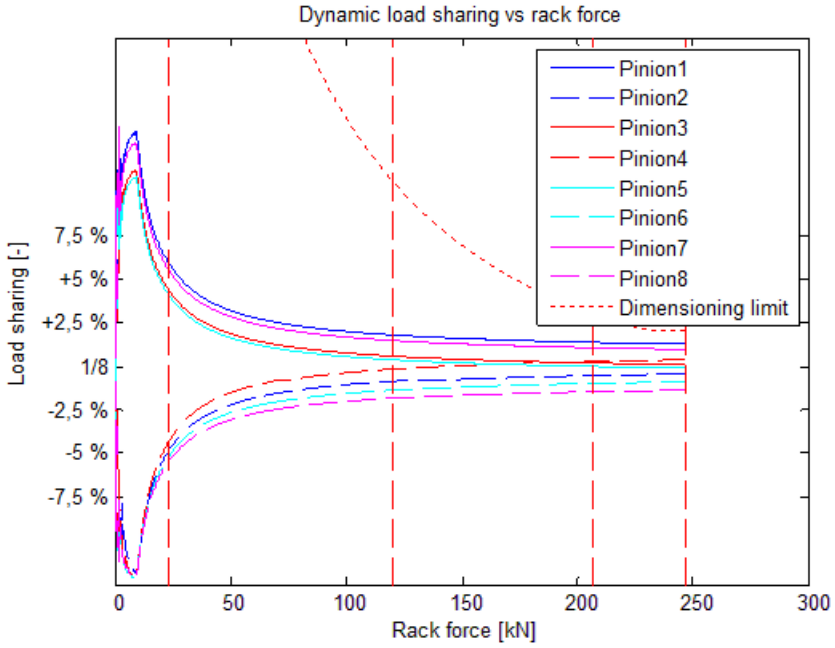

Figure 29. Load sharing plotted against rack load in direction $\vec{B}$.

As identified before the load sharing in direction $\vec{B}$ differs from direction $\vec{A}$ due to the geometrical differences. The difference remaining in direction $\vec{A}$ is due to the difference in stiffness between the flex units further stressing the importance of good control over the flex unit stiffness. Load sharing at different loads in direction $\vec{B}$ is displayed in Table 8.

Table 8. Load sharing in direction $\vec{B}$ for the dynamic model at *120 kN*, *207 kN*, *247 kN*. Perfect load sharing is 1/8=0.125.

Pinion	120 kN	207 kN	247 kN
1	0,1432	0,139	0,138
2	0,1159	0,12	0,121
3	0,1311	0,1272	0,1263
4	0,1236	0,128	0,129
5	0,1291	0,1252	0,1243
6	0,1108	0,1147	0,1156
7	0,1401	0,1349	0,1324
8	0,1062	0,11	0,1108
Mean LS uneven	0,135875	0,131575	0,13025
Mean LS even	0,114125	0,118175	0,1191

Including error tolerances in the model changes both the best possible as well as the momentary load sharing behaviour since the errors are both static and dynamic in character. The load sharing distribution at *247 kN* for the dynamic model show a slightly smaller deviation then the static model even though they are almost identical. None of the 1000 gearboxes in the simulated population fail due to more then *2,5%* overload as seen for pinion 1 in Figure 30. and Appendix B: Additional Figures for the remaining pinions.

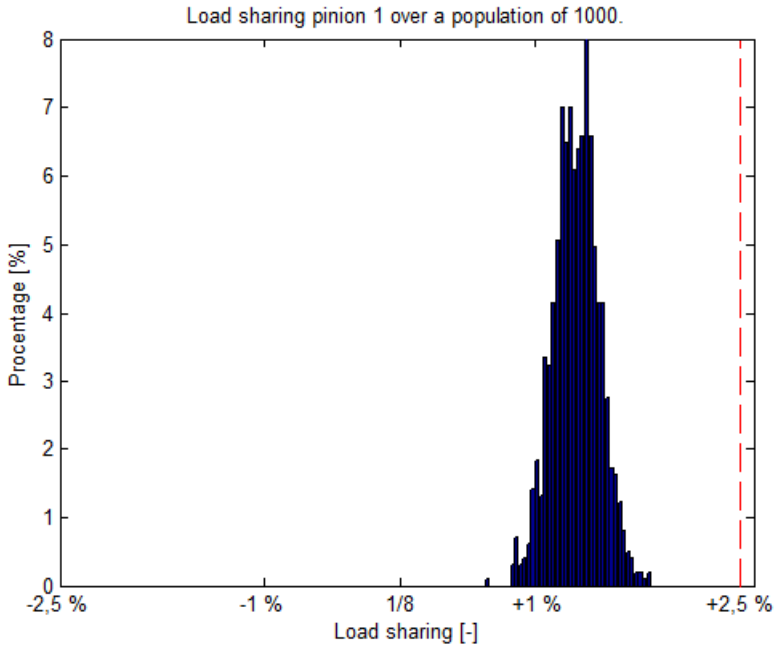

Figure 30. Load sharing for pinion 1 in direction $\vec{B}$ for a population of 1000 gearboxes at *247 kN*. None of the gearboxes fail due to overload of more than *2,5%* of the total load above the nominal *1/8*.

Frequency analysis

Since there are 23 DOF in the dynamic model there is also 23 natural frequencies in the system. However since all gear interactions occur multiple times only 11 are unique, see Table 9.

Table 9. Natural frequencies of the Cascade gearbox based on the dynamic model.

Frequency [Hz]
79210
479210
17374
4737
110
1701
1168
740
2606
991
4632

None of the natural frequencies derived from the dynamic model match that of the input rack load oscillations at *8 Hz*.

4.6 Comparison

A numerical comparison between the physical measurements, static model and dynamic model has to be held at the maximum load achieved during the physical measurements since the extrapolation has to be seen as a type of model in itself. The highest load was registered at *23 kN* during the static tests. Results from these runs will because of that be used for comparison, see Table 10. An added benefit of using the static tests is the less oscillatory behaviour of the results.

Table 10. Load sharing comparison between the static tests, static model and dynamic model at *23 kN*. Perfect load sharing is 1/8=0.125.

	Static measurements		Static model		Dynamic model	
Pinion	$\vec{B}$	$\vec{A}$	$\vec{B}$	$\vec{A}$	$\vec{B}$	$\vec{A}$
1	0,195418	0,132024	0,1807	0,13247	0,1848	0,1332
2	0,078937	0,107797	0,076244	0,12592	0,07589	0,1256
3	0,170688	0,114412	0,16826	0,12109	0,1692	0,1219
4	0,047478	0,142478	0,081434	0,13449	0,08104	0,134
5	0,179358	0,128724	0,16538	0,11901	0,1664	0,12
6	0,076231	0,090939	0,72651	0,11999	0,0726	0,12
7	0,168922	0,175805	0,17974	0,12935	0,1806	0,1303
8	0,082933	0,107821	0,069625	0,11499	0,06956	0,1151
Mean LS uneven	0,1785965	0,13774125	0,17352	0,12548	0,17525	0,12635
Mean LS even	0,07139475	0,11225875	0,23845325	0,1238475	0,0747725	0,123675

Results from the static and dynamic model used for the comparison are derived without error tolerances since results are random with error tolerances included and the chances of hitting the same tolerances as the test rig are unlikely. The effect on load sharing caused by the error

tolerances are presented in an earlier chapter. In addition to that results from the dynamic model are derived with the brake applied to simulate the static measurements and the static model as closely as possible.

The similarity between the static measurements, static models and dynamic models load sharing curves are more easily seen when displayed in the same graph, see Figure 31. Results from the remaining pinions are available in Appendix B: Additional Figures.

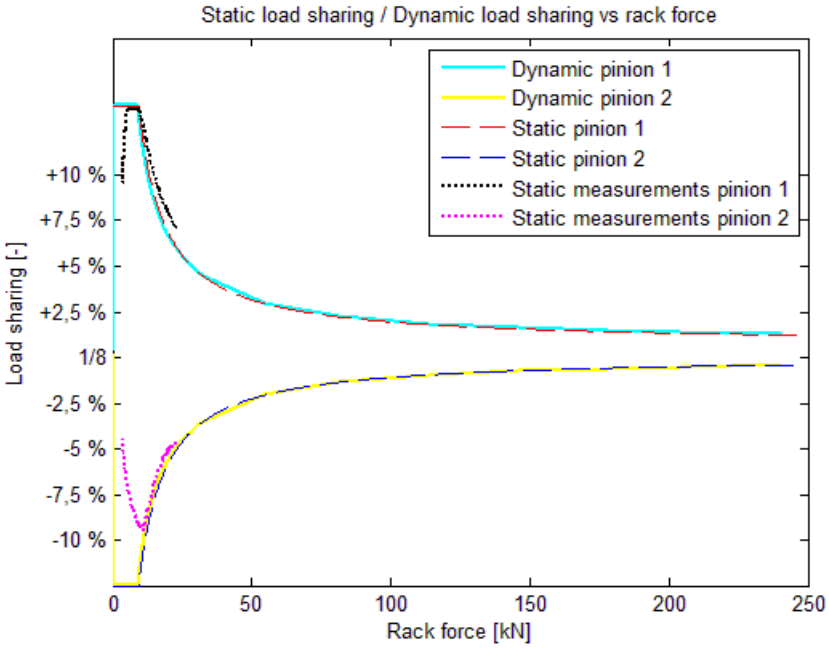

Figure 31. Load sharing curves for pinion 1 and 2 from the static measurements, static model and dynamic model plotted against rack load.

5 DISCUSSION AND CONCLUSIONS

In this chapter a thorough discussion regarding made assumptions and result in this thesis is presented. Also presented are conclusions drawn in respect to the results presented earlier in the thesis.

5.1 Discussion

The difference in load sharing when comparing the measurement and the model results could be explained by the fact that the measurements are done during such low loads that the flex units have not yet entered their linear phase. This means that the pinions taking a smaller load at that time are likely to have higher momentary spring stiffness and more deformation left until they reach their linear phase. This is especially true in direction $\vec{B}$ but is also valid in direction $\vec{A}$. Depending on which pinions this applies to it could possibly give better or worse load sharing depending if it cancels or enhances the already present spring stiffness differences.

The crossing of the load sharing curves was something that was only observed in the models. This is due to the fact that the extrapolation of the measurement values assumed constant load differences between the ideal and the actual load sharing. Since the results is not the same in both instances, that assumption proved faulty although useful to establish approximate values and verify the behaviour of the models. From this it could be concluded that if the load keeps increasing it will eventually reach a load sharing corresponding to 1/8 times the stiffness ratios. This of course assumes that the stiffness of the flex units in fact is linear. This is something that needs further testing and evaluation since it could be expected that the stiffness will not be completely linear during the entire deformation.

As discussed earlier the stiffness ratios have a large effect on the load sharing due to the converging against a value directly proportional to the stiffness ratios. Subsequently a large difference in flex unit stiffness would result in a large load sharing difference. For that reason a narrower stiffness spectrum is beneficial and an important component to have good understanding and specification of. The present specification from the manufacturer of *±20%* does in a worst case scenario when one of the pinions are *20%* stiffer than the mean result in a load sharing which converges against $1.20 \cdot 0.125 = 0.15$ which is right at the dimensioning limit. This calculation is without any concern of geometrical differences or error tolerances.

The approximated linear flex unit stiffness is *34%* higher than the specified value. This could be due to a number of different things. The manufacturer states that it is very hard to accurately control the stiffness of the flex units. In addition to that, modifications made to the flex units during installation could also have affected the end stiffness. It could also be something in the assembly which is obstructing the deformation. Further continuing this reasoning, differences between the approximated flex unit stiffness and the specified value could be due to a too small testing interval. Since the stiffness beyond the measurements is approximated with the help of previous values it must be viewed as a qualified guess rather than an absolute truth. This results in a source of error which if possible should be better determined.

The use of results lacking errors in the comparison between the models and measurements must be seen as a simplification which potentially could change the outcome. However it is a necessary simplification given the fact that it is impossible to determine all errors perfectly. Including errors could both improve and worsen load sharing for specific pinions. As a comparison it is because of this better to exclude errors as it gives a median result.

From the results of the tolerances effect on the load sharing it was observed that none of the gearboxes failed due to more then *2,5%* overload on one pinion in either model. However it was noted that pinion 1 was closest to fail even though it was still safe. This was due to the combination of the second highest flex unit stiffness in one of the uneven pinions. From this it is possible to draw the conclusion that the four stiffest flex units are best fitted to the even pinions and that the flex units remove much of the effect from the error tolerances.

The frequency of the oscillations in the input rack load did not match any of the frequencies derived from the dynamic model. From this the conclusion is that the origin of the vibrations is something outside the gearbox. Since the frequency was low it is most likely the wire transferring force to the rack that is the source.

Simplifications always mean a step away from the reality. In the models they were however necessary to speed up the solution and enable the ode-solver in *MATLAB* to run efficiently. They also served as a boundary to reduce the models size and scope. Most simplifications made in this thesis are supported by scientific articles on gear modelling giving better credibility and assurance of good accuracy. Even though simplifications were made to improve efficiency, computing power was still an issue which required optimization of the codes to avoid too long solution times. Despite this computing time for the population of 1000 gearboxes with the dynamic model reached one and a half days.

Since the models do not correspond exactly with the measurements it is hard to determine their accuracy since the measurements were conducted at such small loads. This is unfortunate however measurements at higher loads would give a clearer understanding of the load sharing behaviour during those conditions. Reaching the point where the load sharing curves first intersect would be a good target since it would provide an additional point for calibration. The fact that both models correspond well with each other does however provide a good indication of their accuracy.

Something that potentially could affect the accuracy of the measurement data is the fact that the load sharing data from the installed sensors are combined from two identical but separate tests. This was due to a hardware problem which prevented all sensors from being connected at the same time. However since the tests were identical, differences between them were small in the same magnitude as the sensor accuracy.

5.2 Conclusions

The results of this thesis have led to number of conclusions regarding the performance and improvement of the Cascade gearbox. The first is that the importance of the accuracy of the flex unit stiffness increase with the load. At high loads when the initial load difference influence over the load sharing is low, the same converges against 1/8 times the stiffness ratio. In the best of worlds full control of a variable stiffness would be the ultimate solution. Also discovered was the previously unknown load sharing behavior in direction $\vec{B}$ due to the geometric differences. This caused the uneven pinions to take higher load initially while the backlash was closed after which the even pinions started taking part of the load.

6 RECOMMENDATIONS AND FUTURE WORK

In this chapter recommendations for future work to evolve and further improve the models are stated together with general recommendations on subjects treated by this thesis.

6.1 Recommendations

Since the stiffness ratio had such an impact on the load sharing, extra effort to decrease the difference in stiffness is recommended. A change in type or method would possibly improve the control of the flex unit stiffness. If the flex unit stiffness had a more linear curve meaning lower stiffness during low loads it would potentially improve the load sharing. Requiring a more exact specification alternatively pre-testing of the flex unit stiffness offers the possibility to mount the four flex units with the lowest stiffness to the uneven pinions resulting in better initial load sharing as well as, although not much, load sharing during high loads. A reduction of the geometric differences would improve the load sharing difference between the uneven and even pinions since this is the cause of the initial difference. In order to reduce the lateral force on the rack induced by the initial load sharing difference between the even and uneven pinions strategically introduced geometric differences could be arranged in such a way that rotational forces on the rack could also be avoided. Also possible would be to introduce geometric differences affecting both directions which would then reduce the difference between the uneven and even pinions by half. The best solution would be to use a method capable of producing a variable stiffness. If implemented it would guarantee perfect load sharing at all times regardless of errors.

6.2 Future work

Future improvements to the models outside of the set delimitations and scope for this thesis include implementation of the gearbox friction and determine the stiffness of the flex units during their entire deformation range. Also possible is to increase the dynamic model to cover three degrees of freedom for each gear. This would allow for further analysis of the gearbox movements during operation. Something that could improve user friendliness is to integrate both models in a GUI controlling the models and providing useful graphs. Additionally it could be useful to control the models the same way as the existing test rig. This would simplify analysis and comparison between the two. Implementing the model in large scale modelling could possibly also be beneficial to simulate the complete WEC. Results from this thesis should finally be used to improve the existing flex unit design. Given the new data collected from the models it would also be possible to conduct lifetime analysis of the flex units. In order to improve accuracy of those results, testing of the flex unit’s stiffness during their complete deformation cycle is the number one priority.

7 REFERANCES

Ashino R. Nagase M. and Vaillancourt R., *"Behind and Beyond the MATLAB ODE Suite"*, Computers & Mathematics with Applications, 40.4, 2000, pp 491-512.

Babarit A. Duclos G. and Clément A.H., "Comparison of latching control strategies for heaving wave energy device in random sea", Applied Ocean Research, Vol. 26, 2004, pp 227-238.

Bodas A. and Kahraman A., *"Influence of Carrier and Gear manufacturing Errors on the Static Load Sharing Behavior of Planetary Gear Sets"*, JSME International Journal, Vol. 47, 2004, pp 908-915.

Chen Y. and Wu x., *"Dynamic Load Sharing Behavior of Planetary Gear Train with Backlashes"*, International Conference on Engineering Computation, 2009, pp 209-212.

Clément A. et al., *"Wave energy in Europe: current status and perspectives"*, Renewable and Sustainable Energy Reviews, Vol. 6, 2002, pp 405-431.

CorPower Ocean, *"The CorPower Wave Energy Converter"*, http://www.corpowerocean.com/corpower-technology/corpower-wave-energy-converter/, accessed 2015-02-12, 2012.

Dunn O. and Clark V., *"Basic Statistics: A Primer for the Biomedical Sciences"*, Fourth Edition, John Wiley & Sons Ltd, Chichester, 2009.

EIA (U.S. Energy Information Administration), *"International Energy Statistics"*, http://www.eia.gov/cfapps/ipdbproject/iedindex3.cfm?tid=6&pid=117&aid=12&cid=regions&syid=2008&eyid=2012&unit=BKWH, accessed 2015-02-12, 2012.

Falnes J., *"A review of wave-energy extraction"*, Marine Structures, Vol. 20, 2007, pp 185-201.

Fernandez A. Viadero F. Iglesias M. García P. de-Juan A. and Sancibrian R., *"A model for study of meshing stiffness in spur gear transmissions"*, Mechanism and Machine Theory, Vol. 61, 2013, pp 30-58.

Fisher B., *"Mechanical Tolerance Stackup and Analysis"*, Second Edition, Taylor & Francis Group, Boca Raton, 2011.

Hals J., *"Modelling and phase control of wave-energy converters"*, Thesis for the degree of philosophiae doctor, Norwegian University of Science and Technology, 2010.

Jelaska D., *"Gears and gear drives"*, John Wiley & Sons Ltd, Chichester, 2012.

Kahraman A. Kharazi A.A. and Umrani M., "*A deformable body dynamic analysis of planetary gears with thin rims"*, Journal of Sound and Vibration, Vol. 262, 2003, pp 752-768.

Kahraman A., *"Free torsional vibration characteristics of compound planetary gear sets"*, Mechanism and Machine Theory, Vol. 36, 2001, pp 953-971.

Kahraman A., *"Load Sharing Characteristics of Planetary Transmissions"*, Mechanical Machine Theeory, Vol. 29, 1994a, pp 1151-1165.

Kahraman A., *"Planetary Gear Train Dynamics"*, Journal of Mechanical Design, Vol. 116, 1994b, pp 713-720.

Kahraman A., *"Static Load Sharing Characteristics of Transmission Planetary Gear Sets: Model and Experiment"*, Transmission and Driveline Systems Symposium, 1999.

Kvam P. and Vidakovic B., *"Nonparametric Statistics with Applications to Science and Engineering"*, John Wiley & Sons Ltd, Chichester, 2007.

Lallement G. and Inman D., *"A Tutorial on Complex Eigenvalues"*, Proceedings-Spie The International Society for Optical Engineering, 1995, pp 490-495.

Lim T.C and Li J., *"Dynamic Analysis of Multi-Mesh Counter-Shaft Transmission"*, Journal of Sound and Vibration, Vol. 219, 1999, pp 905-919.

Moradi H. and Salarieh H., "A*nalysis of nonlinear oscillations in spur gear pairs with approximated modelling of backlash nonlinearity"*, Mechanism and Machine Theory, Vol. 51, 2012, pp 14-31.

Oberg E. Jones F. Horton H. and Ryffel H., *"Machinery´s Handbook"*, 28th Edition, Industrial Press INC, New York, 2008.

Peng Z. and Wu S., *"Influence of Central Members Radial Support Stiffness on Load Sharing Characteristics of Compound Planetary Gearsets"*, American Gear Manufacturers, Fall Technical Meeting, 2014, pp 43-52.

Rao Z. et al., *"Nonlinear torsional instabilities in two-stage gear systems with flexible shafts"*, International Journal of Mechanical Sciences, Vol. 82. 2014, pp 60-66.

Somvir A. Sachin K. and Viney J., *"Application of Monte Carlo Technique for Analysis of Tolerance & Allocation of Reciprocating Compressor Assembly"*, International Journal of Research in Mechanical Engineering & Technology, Vol. 2, 2012, pp 15-20.

Spearman C. *"The Proof and Measurement for Association Between Two Things"*, American Journal of Psychology, Vol. 15, 1904, pp 72-101.

Vicinanza D. Contestabile P. and Ferrante V., *"Wave energy potential in the north-west of Sardinia (Italy)"*, Renewable Energy, Vol. 50, 2013, pp 506-521.

Woolson R. and Clarke W., *"Statistical Methods for the Analysis of Biomedical Data"*, Second Edition, John Wiley & Sons Ltd, Chichester, 2002.

Zhu B. Chen X. and Zhou L., *Dynamic Simulation of the Meshed Gears Based on ADAMS"*, Materials Science Forum, Vols. 800-801, 2014, pp 708-711.

APPENDIX A: MATRIX REPRESENTATIONS

$$F_m(t) = \begin{bmatrix} f_{input} \\ 0 \\ -f_{generator} \\ 0 \\ \vdots \\ 0 \end{bmatrix}$$

$$C(t) = \begin{bmatrix}
C_r & 0 & 0 & 0 & 0 & 0 & -c_{rp1} & 0 & -c_{rp2} & 0 & 0 \\
0 & C_o & -c_{G314} & -c_{G324} & 0 & 0 & 0 & 0 & 0 & 0 & -c^{h}_{sG4f} \\
0 & -c_{G314} & C_{G31} & 0 & -r_{G2}r_{G3}\cdot c_{s2131} & 0 & 0 & 0 & 0 & 0 & 0 \\
0 & -c_{G324} & 0 & C_{G32} & 0 & -r_{G2}r_{G3}\cdot c_{s2232} & 0 & 0 & 0 & 0 & 0 \\
0 & 0 & -r_{G2}r_{G3}\cdot c_{s2131} & 0 & C_{G21} & 0 & 0 & -c_{G1121} & 0 & 0 & 0 \\
0 & 0 & 0 & -r_{G2}r_{G3}\cdot c_{s2231} & 0 & C_{G22} & 0 & 0 & 0 & 0 & 0 \\
-c_{rp1} & 0 & 0 & 0 & 0 & 0 & C_{p1} & -r_p r_{G1}\cdot c_{f1} & 0 & 0 & 0 \\
0 & 0 & 0 & 0 & -c_{G1121} & 0 & -r_p r_{G1}\cdot c_{f1} & C_{G11} & 0 & -c_{G1211} & 0 \\
-c_{rp2} & 0 & 0 & 0 & 0 & 0 & 0 & 0 & C_{p2} & -r_p r_{G1}\cdot c_{f2} & 0 \\
0 & 0 & 0 & 0 & 0 & 0 & 0 & -c_{G1211} & -r_p r_{G1}\cdot c_{f2} & C_{G12} & 0 \\
 & & & & & & & & & & \ddots \quad 0 \\
0 & -c^{h}_{sG4f} & 0 & 0 & 0 & 0 & 0 & 0 & 0 & 0 & 0 \quad C_f
\end{bmatrix}$$

APPENDIX B: ADDITIONAL FIGURES

Pitch deviation from Tolerance analysis.

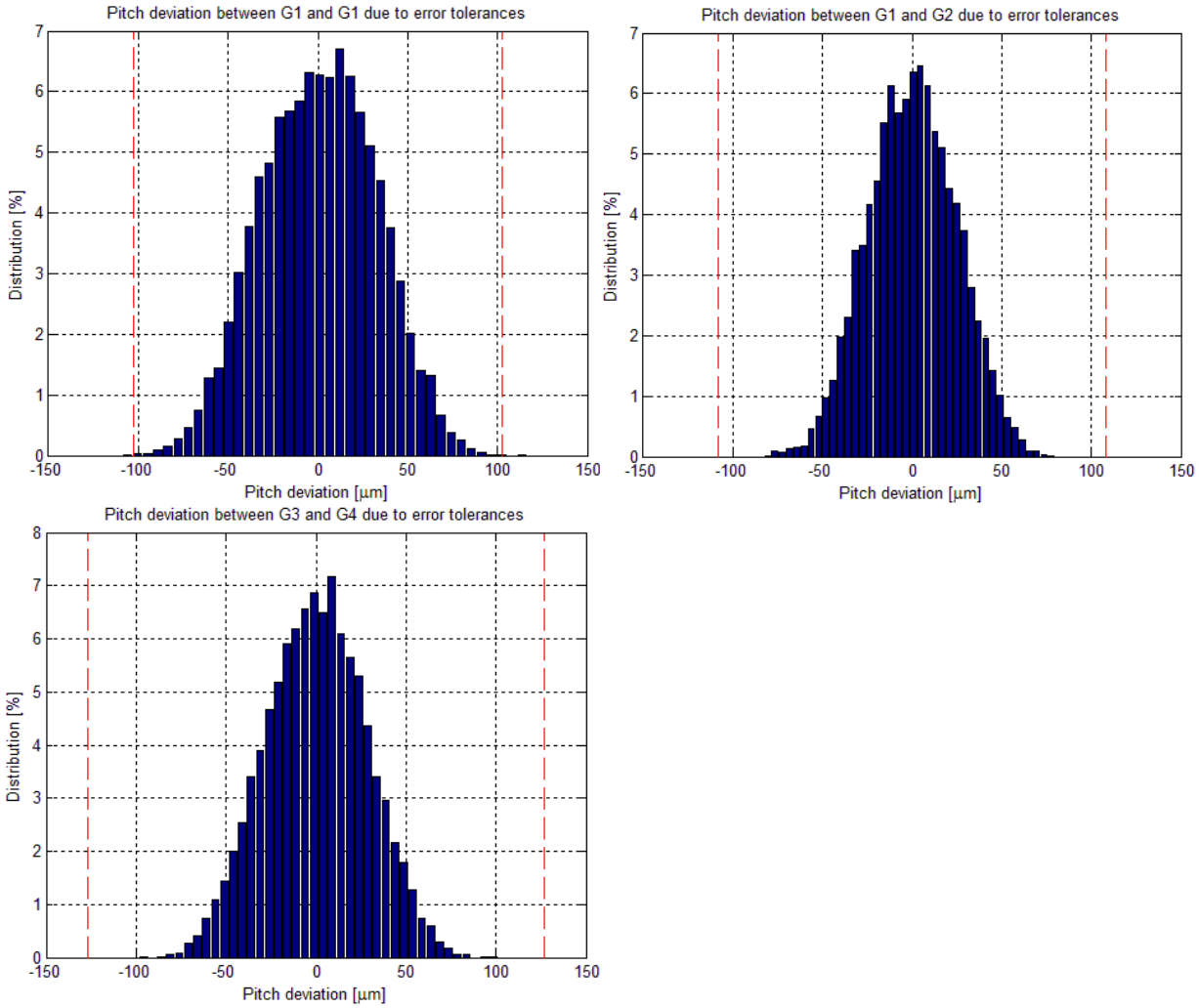

Flex unit stiffness from Stiffness measurement.

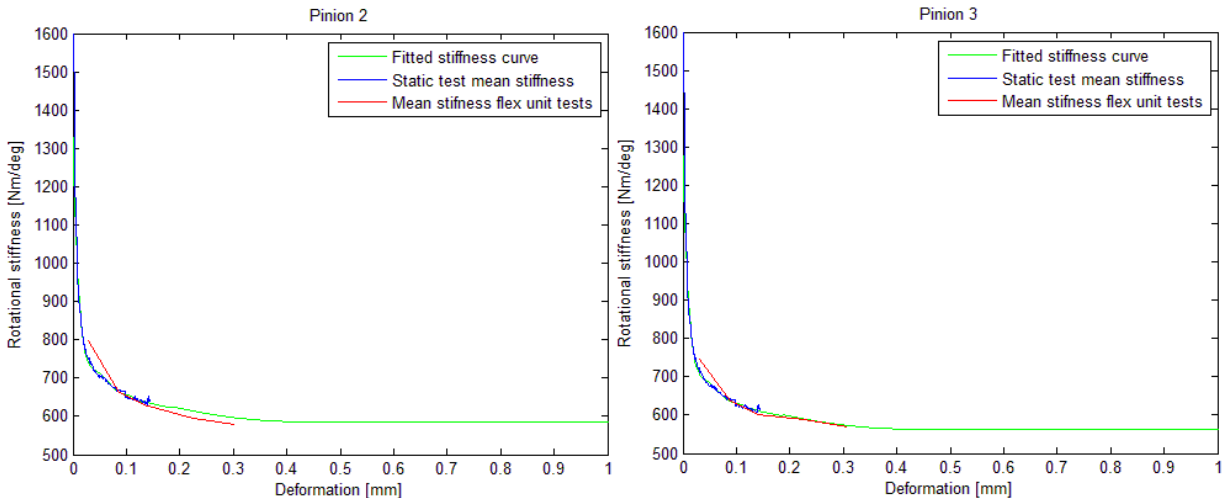

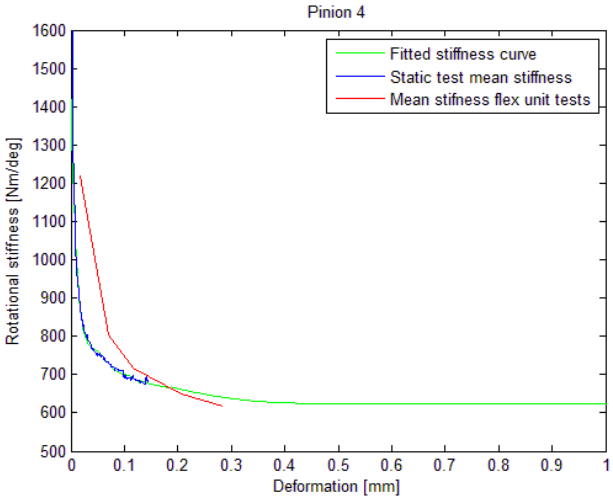
Pinion 4
Fitted stiffness curve
Static test mean stiffness
Mean stifness flex unit tests
Rotational stiffness [Nm/deg]
Deformation [mm]

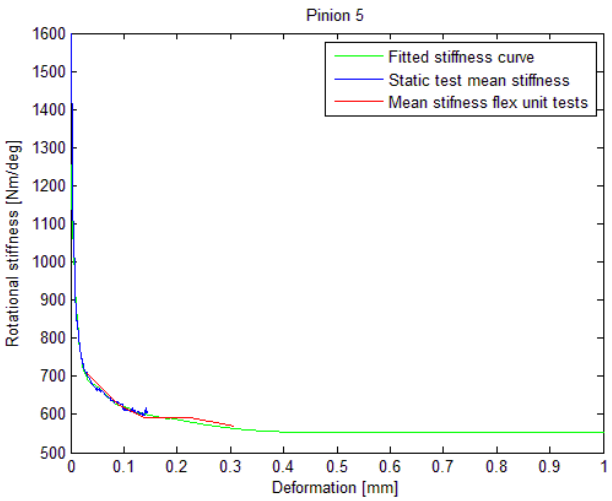
Pinion 5
Fitted stiffness curve
Static test mean stiffness
Mean stifness flex unit tests
Rotational stiffness [Nm/deg]
Deformation [mm]

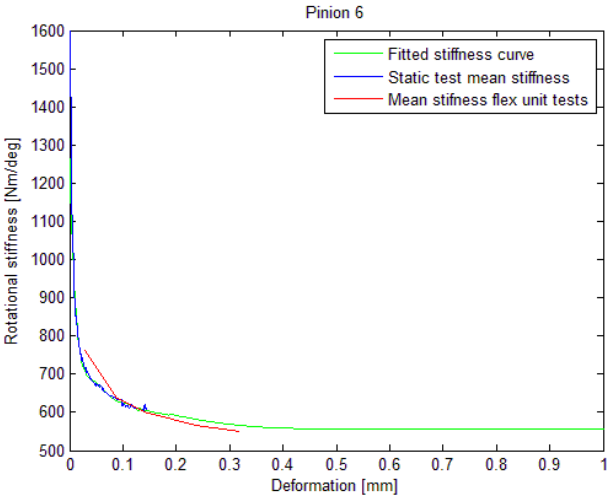
Pinion 6
Fitted stiffness curve
Static test mean stiffness
Mean stifness flex unit tests
Rotational stiffness [Nm/deg]
Deformation [mm]

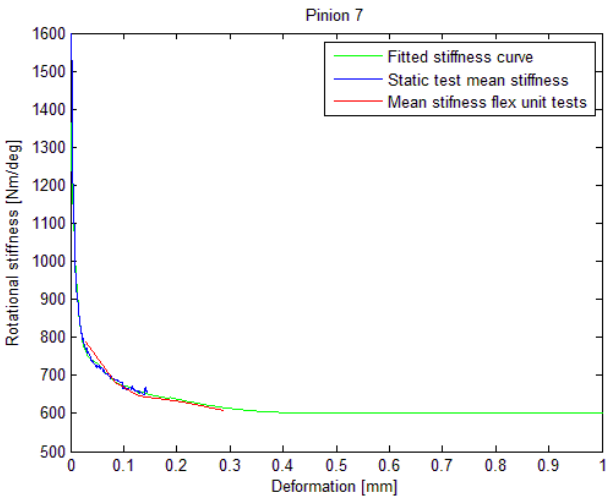
Pinion 7
Fitted stiffness curve
Static test mean stiffness
Mean stifness flex unit tests
Rotational stiffness [Nm/deg]
Deformation [mm]

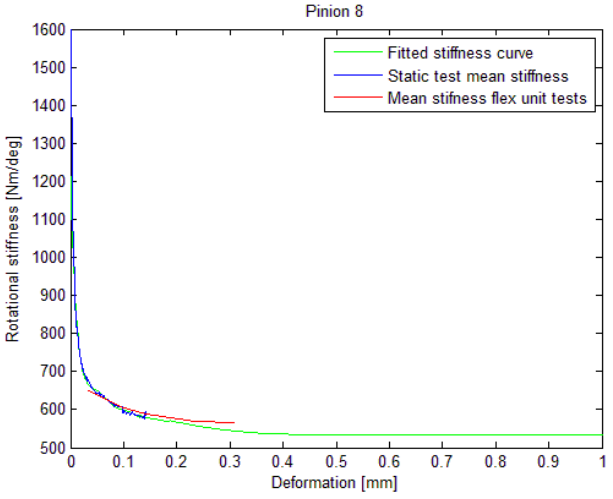
Pinion 8
Fitted stiffness curve
Static test mean stiffness
Mean stifness flex unit tests
Rotational stiffness [Nm/deg]
Deformation [mm]

Load sharing with errors from Static model.

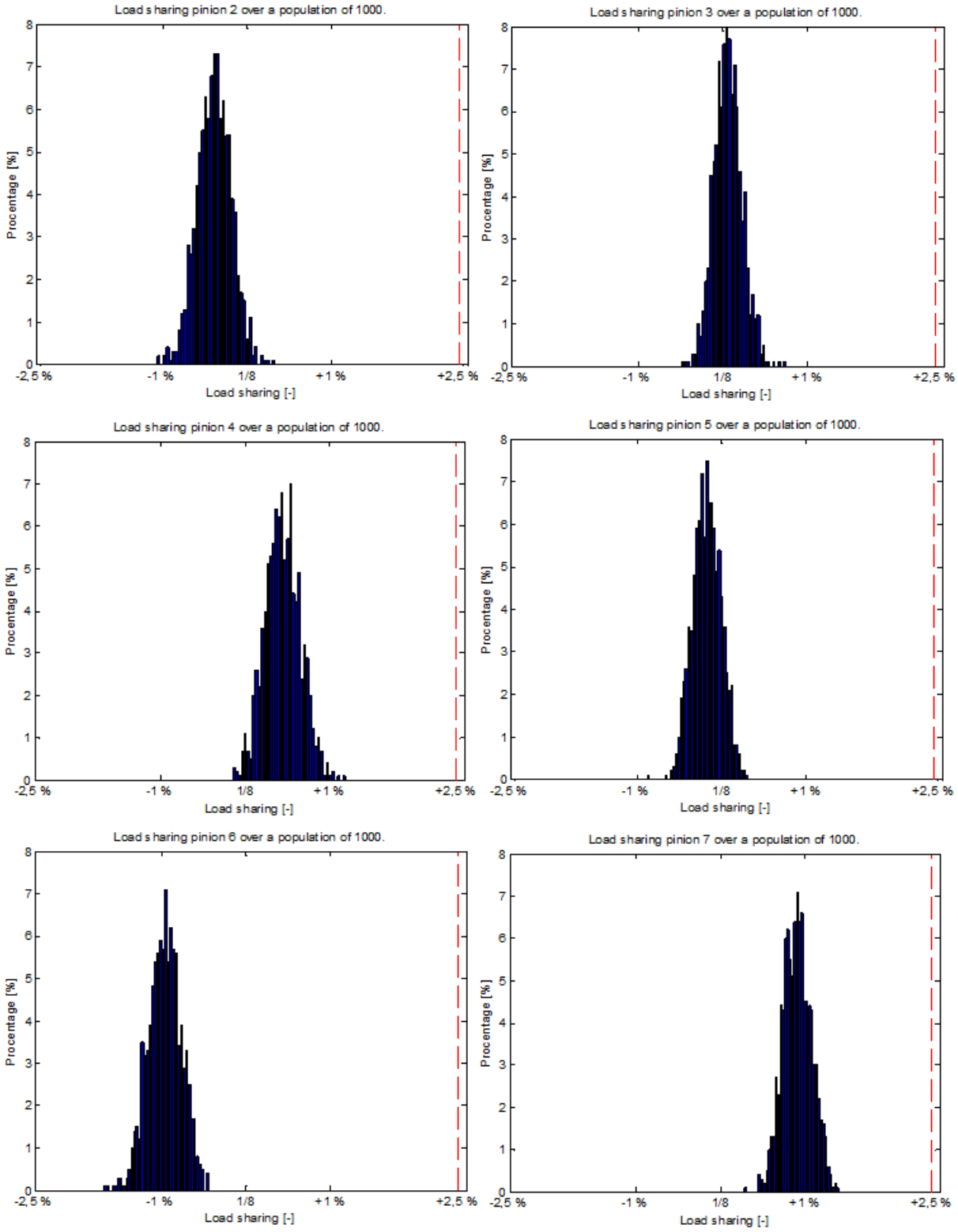

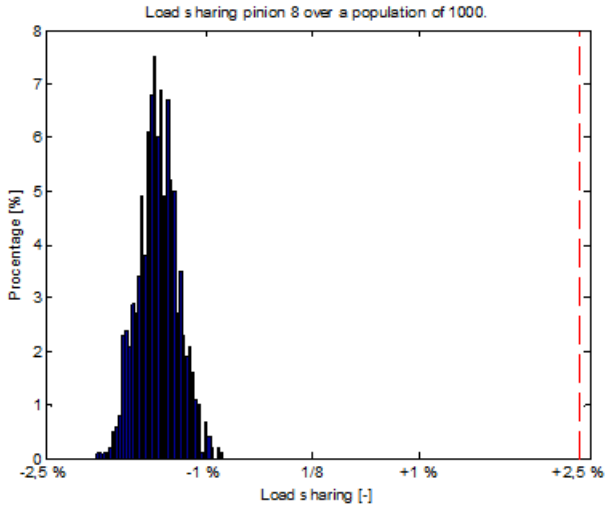

Load sharing with errors from Dynamic model.

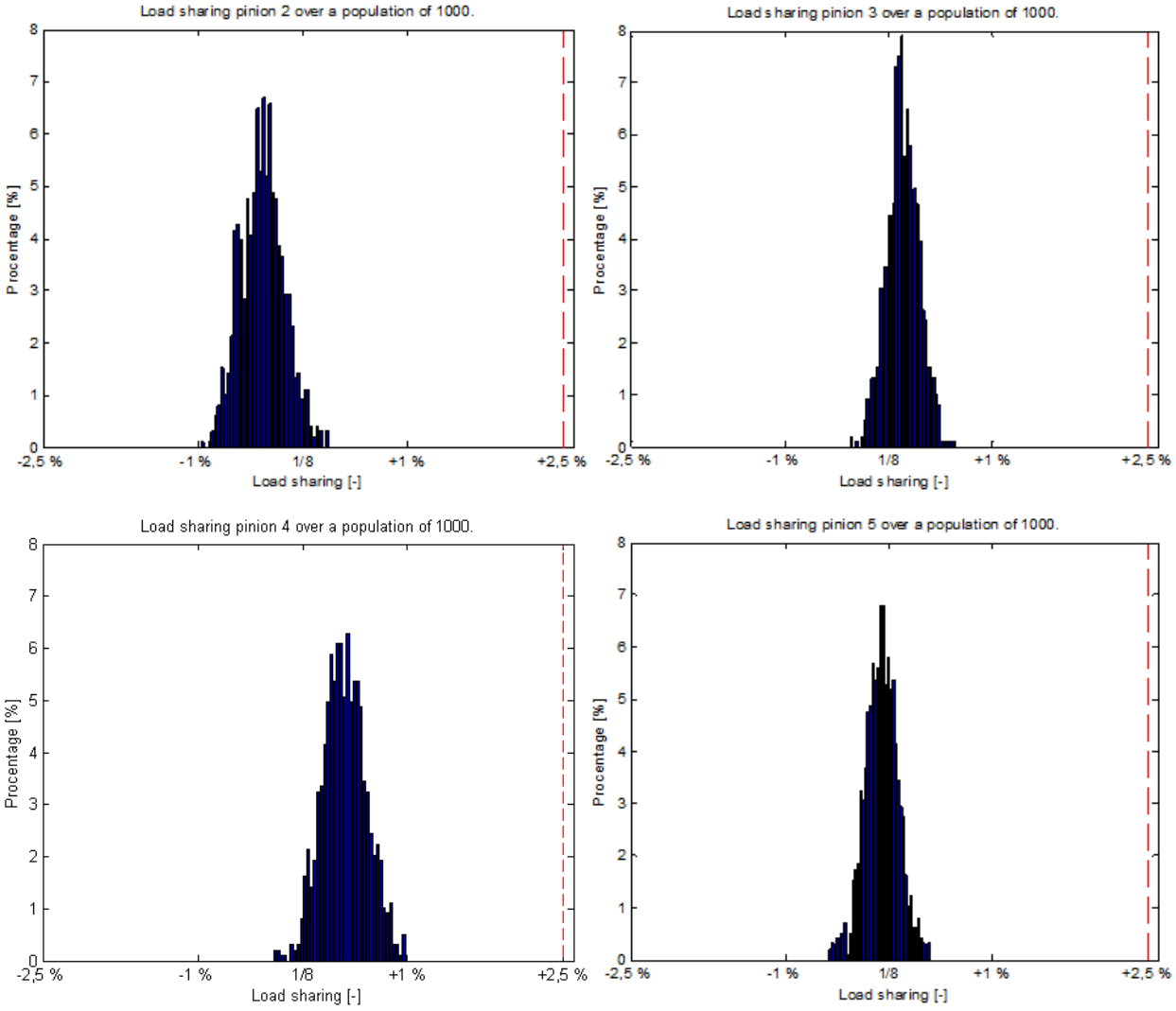

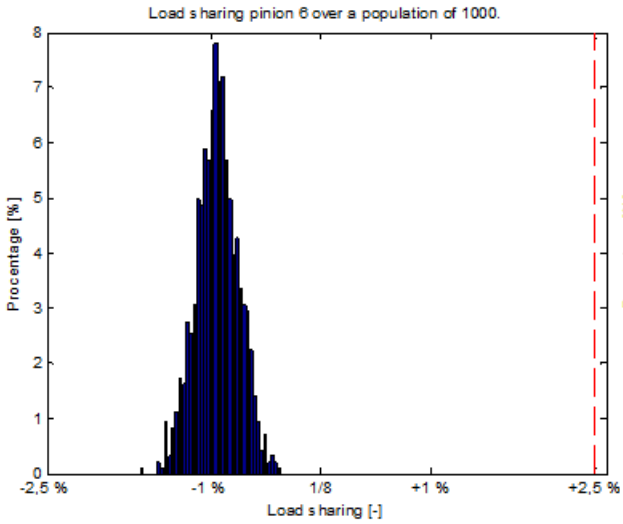
Load sharing pinion 6 over a population of 1000.
Procentage [%]
Load sharing [-]
-2,5 %
-1 %
1/8
+1 %
+2,5 %

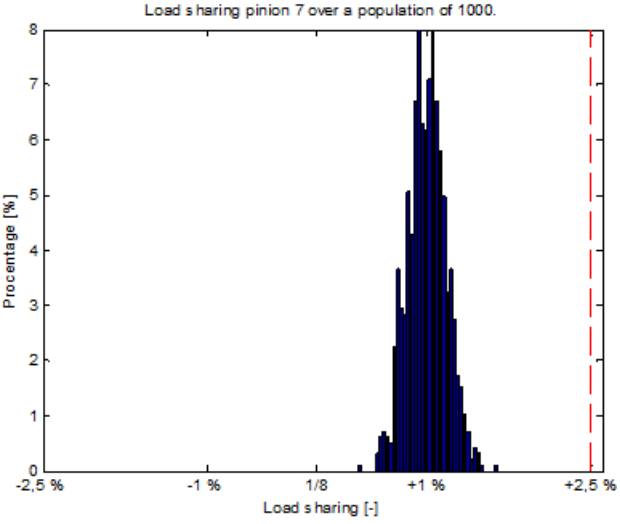
Load sharing pinion 7 over a population of 1000.
Procentage [%]
Load sharing [-]
-2,5 %
-1 %
1/8
+1 %
+2,5 %

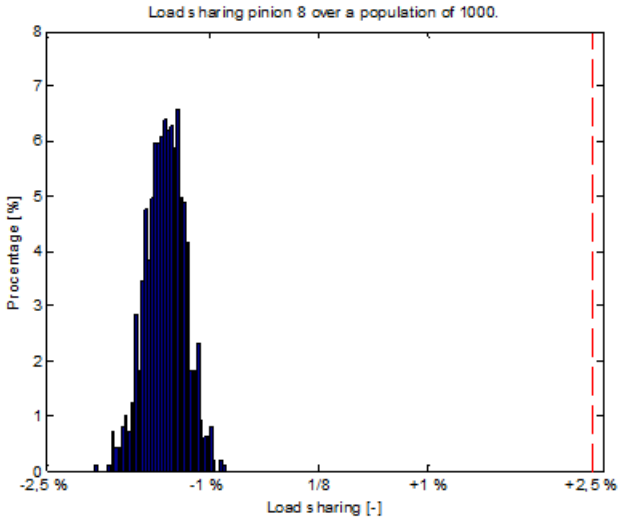
Load sharing pinion 8 over a population of 1000.
Procentage [%]
Load sharing [-]
-2,5 %
-1 %
1/8
+1 %
+2,5 %

Combined load sharing curves static and dynamic model from Comparison.